Centrosome Loss in Embryonic Development Disrupts Axonal Pathfinding and Muscle Integrity

Beatriz González[1,2], Júlia Sellés-Altés[1], Jèrica Pla-Parron[1], Judith Castro-Ribera[1], and Sofia J. Araújo*[1,2]

[1]Department of Genetics, Microbiology and Statistics, Facultat de Biologia, Universitat de Barcelona (UB), 08028 Barcelona, Spain

[2]Institut de Biomedicina Universitat de Barcelona (IBUB), Barcelona, Spain

*Corresponding author. email: S. J. Araújo sofiajaraujo@ub.edu,

Keywords: centriole; centrosome; axon; nervous system; muscle; Drosophila; Sas-4; Sas-6; wiggliness, tortuosity

Running title: centriole loss disrupts axon and muscle development

Abstract

Centrosomes, the primary microtubule-organizing centres (MTOCs), are crucial for early neuronal development, particularly in establishing polarity and promoting axon formation. Once thought dispensable in many terminally differentiated cells, growing evidence shows that many cells retain active centrosomes, while others do not, highlighting context-dependent roles in specialized functions. In some mammalian neurons, centrosome-mediated microtubule (MT) remodelling is essential for axon elongation, with centrosome dysfunction leading to axonal misrouting and growth defects. Although active centrosomes have been detected in embryonic tracheal terminal cells of *Drosophila melanogaster*, their activity in neurons *in vivo* has not been observed. Their gradual loss during embryogenesis has been reported as non-essential for organogenesis, as adult flies can eclose without centrioles.

To investigate centrosome activity in neurons, we revisited *Drosophila Sas-4* mutants, which exhibit centrosome loss (CL), and observed that 50% of homozygous mutant individuals fail to hatch as larvae. We analysed their development, focusing on the expressivity and penetrance of nervous system phenotypes, and examined centrosome localization in neurons. Our findings confirm the presence of centrosomes in wild-type motor and sensory neurons in *Drosophila* and their localization near the nascent axon in motor neurons. CL conditions resulted in axonal misrouting and muscle developmental abnormalities. Targeted downregulation of Sas-4 in the pioneer motor neurons aCC, pCC and RP2 induced axon guidance errors, indicating an autonomous role for centrosomes in axonal navigation. Colocalization of acetylated- and γ-tubulin with centrosomes in motor neurons and MT repolymerization analysis further confirmed the presence of active centrosomes in these cells. Analysis of motor axons revealed that CL leads to motor axon tortuosity, a characteristic associated with neurodegeneration. This is the first direct association of CL with axonal morphological phenotypes, highlighting the role of centrosomes in neuronal development and their broader influence on nervous system structure and function.

Introduction

Centrosomes are small membrane-less organelles that serve as primary microtubule-organizing centres (MTOCs). Composed of a mother-daughter centriole pair surrounded by pericentriolar material (PCM), they anchor and nucleate microtubules (MTs) through γ-tubulin ring complexes (γ-TuRCs) (Bettencourt-Dias & Glover, 2007). During mitosis, centrosomes organize the spindle apparatus, while their role in interphase is more variable (Conduit *et al*, 2015). Abnormalities in centrosomes are linked to disorders like microcephaly and neurodevelopmental disorders, highlighting the importance of centrosome function in early neurodevelopment (Goundiam & Basto, 2020; Marthiens *et al*, 2013). However, how centrosome numbers affect differentiated cells and their involvement in post-cell-division organogenesis is not yet fully understood. Although traditionally studied in dividing cells, recent

insights suggest centrosomes also regulate cellular behaviours in differentiated cells, contradicting the assumption that centrosome-based MTOCs are largely inactive in such contexts.

In vertebrates, centrosomes are critical for embryonic development, often because they are tightly linked to checkpoint controls that ensure accurate cell division and developmental progression (Meyer-Gerards & Bazzi, 2025). Null mutations in mouse *Cenpj* (also called *Sas4*) lead to centriole loss and embryonic arrest at embryonic day 9, and *Sass6*-mutant mouse embryos arrest at mid-gestation (Bazzi & Anderson, 2014; Grzonka & Bazzi, 2024). In contrast, *Drosophila melanogaster* embryos have been reported to develop to adulthood using maternally supplied Sas-4 and Sas-6, despite gradual centrosome loss (CL) (Basto *et al*, 2006; Fatalska *et al*, 2021; Gogendeau & Basto, 2010). However, these adults are sterile, uncoordinated, unable to form cilia, and die shortly after eclosion (Basto *et al.*, 2006). Without maternal Sas-4, Sas-4 and Asterless (Asl) *Drosophila* embryonic development arrests early (Stevens *et al*, 2007; Varmark *et al*, 2007), as observed in *C. elegans Sas-4* mutants (Leidel & Gönczy, 2003). In *Drosophila* neural progenitor and epithelial cells, centrosome absence impairs spindle assembly and orientation, leading to defects like neural apoptosis and altered brain size, mimicking either human microcephaly or tumourigenesis (Basto *et al.*, 2006; Castellanos *et al*, 2008; Poulton *et al*, 2014; Poulton *et al*, 2017).

Centrosomes are also important for differentiated cellular functions. In mouse fibroblasts, myoblasts and endothelial cells, centrosome position is important for nuclear positioning and cell migration (Chang *et al*, 2015; Gomes *et al*, 2005; Kushner *et al*, 2014). During kidney development, CL leads to decreased branching morphogenesis and small dysplastic kidneys at birth (Cheng *et al*, 2023). In *Drosophila* tracheal terminal cells (TCs), centrosome numbers influence the formation of subcellular lumina during tubulogenesis (Ricolo *et al*, 2016). Increasing centrosome numbers or depleting centrosomal proteins alters this process, stressing centrosome importance in cells with specialized architectures (Ricolo *et al*, 2021).

In some neurons, centrosomes play critical roles as MTOCs during early development, particularly in axon formation, a process reliant on microtubule remodelling to establish

83 neuronal polarity (Meka *et al*, 2022). However, other neuronal types need centrosomal
84 microtubule nucleation for migration but not axon formation (Vinopal *et al*, 2023). In
85 mammalian neurons, centrosomes nucleate MTs in the soma, which are subsequently
86 severed and transported into neurites via motor-driven sliding, enabling axon elongation and
87 polarity establishment (Ahmad & Baas, 1995; del Castillo *et al*, 2015; Stiess *et al*, 2010; Yu *et*
88 *al*, 1993). In hippocampal neurons *in vitro,* suppression of centrosome-mediated functions
89 prevents axonal growth and neurons with more than one centrosome sprout more than one
90 axon (Anda *et al*, 2005). In addition, aberrant centrosome localization, leads to misplaced
91 axonal outgrowth (Anda *et al*, 2010). In human iPSC-derived neurons, depleting centrioles
92 causes significant axonal defects, including mislocalization of axonal MT-associated proteins
93 and affected growth cone morphologies (Lindhout *et al*, 2021). However, as neurons mature,
94 γ-tubulin (γ-tub) remains essential, but centrosomes lose MTOC activity and become
95 dispensable in mammals and flies (Leask *et al*, 1997; Nguyen *et al*, 2011; Sanchez-Huertas
96 *et al*, 2016; Stiess *et al.*, 2010).
97 These findings collectively suggest that while centrosomes are essential in specific cells,
98 stages and contexts, many differentiated cells can adapt to their loss through alternative
99 MTOCs. However, in many cases, CL induces phenotypes which indicate its important function
100 in cytoskeletal remodelling and the acquisition of specialised cell shapes (Araújo, 2019).
101 To investigate the role of centrosomes in neuronal development, we revisited *Drosophila Sas-*
102 *4* mutants with reduced centriole numbers and analysed their embryonic development. We
103 quantified the expressivity and penetrance of nervous system phenotypes and examined
104 centriole localization within neurons. Our findings indicate that loss of centrosomal protein
105 function results in variable expressivity and penetrance of embryonic phenotypes, which likely
106 accounts for inconsistencies in previously reported results. We observed that centrosomes
107 are present and active in *Drosophila* motor and peripheral nervous system (PNS) neurons.
108 Importantly, CL during embryogenesis leads to axonal misrouting and abnormalities in muscle
109 development, emphasising a critical role of centrosomes in proper nervous system and muscle

110 structure formation. To confirm centrosome importance for neuronal cell-shape changes, we
111 were able to specifically observe axonal phenotypes associated with CL.
112
113 **Results**
114
115 ***Sas-4* mutant conditions induce axonal misrouting phenotypes**
116 Spindle assembly abnormal 4 (Sas-4) protein is essential for centriole replication in *Drosophila*
117 and early embryonic development (Basto *et al.*, 2006; Stevens *et al.*, 2007). However, in
118 contrast to *Sas-4* maternal mutants, *Sas-4* zygotic mutant embryos initially progress through
119 early development due to the maternal contribution, gradually losing centrioles during
120 embryonic and larval stages. This progressive centriole loss makes these mutants an excellent
121 model for studying the role of centrosomes in differentiated cells. By embryonic stages 15–16,
122 centrioles have been reported to be undetectable in 50–80% of cells (Basto *et al.*, 2006). By
123 these stages, *Sas-4* mutant embryos exhibit defects in tracheal subcellular lumen formation,
124 showing the importance of centrioles in some differentiated cells (Ricolo *et al.*, 2016).
125 Nevertheless, *Sas-4* homozygous mutants have been reported to reach adulthood, yet, they
126 exhibit early lethality soon after eclosion (Basto *et al.*, 2006). This early adult lethality suggests
127 a critical role for Sas-4 in maintaining cellular and developmental processes essential for
128 organismal viability.
129 To investigate the role of centrosomes in embryonic development, we first analysed the
130 viability of *Sas-4* loss-of-function (LOF) mutants during embryonic, larval and adult stages. As
131 previously reported, we were able to raise *Sas-4* mutant adults; however, only a proportion of
132 Sas-4 individuals were found to eclose. These mutants were uncoordinated and became
133 trapped in the food upon eclosion. When isolated at the pupal stage and placed in Petri dishes,
134 they were able to eclose and survive for longer, but with available food, they died within 24-36
135 hours, which is significantly less than the reported survival rates of unfed flies (2-3 days)
136 (Kopeć, 1928; Pearl & Parker, 1921). These adult individuals exhibited severe motor

137 impairments, barely moving and failing to extend their wings (Fig. 1A). To obtain survival rates,
138 we quantified the percentage of *Sas-4* mutants that reached adulthood, compared to the total
139 number expected, based on Mendelian proportions, from a cross between heterozygous *Sas-*
140 *4*/*TM3twiGFP* individuals and a cross between *Sas-4*/*TM3twiGFP* and a balanced deficiency,
141 which uncovers the *Sas-4* locus (*Df(3R)BSC221/TM3twiGFP*). Since the homozygous
142 balancer chromosome embryos are early embryonic lethal, we could detect a proportion of
143 33.3% mutant embryos surviving to embryonic stage 16, corresponding to all *Sas-4*
144 homozygous embryos. However, we only detected 16.7% of *Sas-4* homozygous L1 larvae 36h
145 after egg laying (AEL) (Fig. 1B, n=407), corresponding to 50% of all *Sas-4* homozygous
146 embryos. This proportion was maintained to wandering L3, pupal and adult stages, suggesting
147 that once the barrier of embryonic stages is passed, centrosomes are no longer necessary for
148 viability, and individuals can reach adult stages as previously reported (Basto *et al.*, 2006).
149 Nevertheless, our results show that only 50% of the *Sas-4* homozygous embryos (16.7% of
150 the total number of individuals, n= 407) successfully reached the larval and adult stages,
151 indicating that CL induces embryonic lethality in the remaining 50% of cases. Although we
152 used a *Sas-4* mutant chromosome from which all other mutations had been removed by
153 recombination, we also assessed the viability of a transheterozygous combination of *Sas-4*
154 and a deficiency that uncovers the *Sas-4* genomic region. Transheterozygous individuals
155 reached adulthood at a rate of 14.6% (n = 337, Fig. 1B), a result comparable to that observed
156 in *Sas-4* homozygotes and confirming this lethality in *Sas-4* null conditions.
157 We then asked if the *Sas-4* embryos exhibited mutant nervous system phenotypes. To do so,
158 we first analysed FasII positive neurons focusing on the trajectories of their motor axons,
159 particularly on the Intersegmental Nerve (ISN) (Fig. 1C). The penetrance of the ISN phenotype
160 was 52.8% (n=53) quantified as at least 2 defects per embryo, despite variability in the
161 expressivity of the phenotype (Fig. 1E and H and Sup. Fig. 1B and K), which agrees with the
162 larval viability observed. The aberrant pathways included the following: synaptic phenotypes,
163 which were evident when the nerve fibres innervated the wrong target or failed to innervate
164 (Fig. 1E and Sup. Fig. 1B, arrow); misrouting phenotypes, which involved defects in nerves

165 that do not follow the wild-type (wt) stereotypical routes (Fig. 1E and Sup. Fig. 1B, asterisk);
166 and crossing phenotypes, which included aberrant crossing between segments (Fig. 1E
167 arrowhead). The same type of anomalous phenotypes was detected in *Sas-4/Df* mutant
168 embryos (Fig. 1F and H), penetrance 56% (n=25), as well as RNAi *Sas-4* downregulation (Fig.
169 1G and H), penetrance 33.3% (n=15). We downregulated Sas-4 using a *UAS-Sas-4RNAi*
170 expressed in all post-mitotic neurons, by an elavGal4 driver (Sup. Fig. 1 D and K) and
171 specifically in a subset of neurons, such as the anterior corner cell (aCC), posterior corner cell
172 (pCC) and RP2 pioneers, using RN2-Gal4 (Fujioka *et al*, 2003). Interestingly, when Sas-4 was
173 specifically downregulated only in these neurons, we observed an additional phenotype:
174 fasciculation/defasciculation defects (Fig. 1G arrow) ISN misrouting and defasciculation
175 phenotypes (Fig. 1G and Sup. Fig. 1K, asterisks and arrowhead). In addition, we observed
176 shorter nerve extensions (Fig. 1G, dot), also observed in some *Sas-4* and *Sas-4/Df* mutant
177 embryos (Fig. 1F' and Sup. Fig. 1C). This suggested these motor axon phenotypes were
178 induced cell-autonomously. We confirmed these downregulation results, using a different
179 RNAi line and could observe similar types of phenotypes (Sup. Fig. 1M-O). Ubiquitous
180 expression of *Sas-4* using a *pUbqSas-4* insertion (Peel *et al*, 2007), could partially rescue the
181 mutant phenotypes, particularly by reducing the number of defects (Fig. 1H and Sup. Fig. 1 E
182 and K).
183 We followed by analysing the peripheral nervous system (PNS) phenotypes of *Sas-4* mutant
184 conditions specifically focusing on their axonal misrouting phenotypes. We could detect axonal
185 misrouting phenotypes in all three mutant conditions: *Sas-4* (penetrance 60% n=20), *Sas-4/Df*
186 (penetrance 55% n=20) and *UAS-Sas-4RNAi* (penetrance 60% n=20) (Fig. 1J-L and M, Sup.
187 Fig. 1F-J) expressed in PNS neurons using *P0163Gal4* (Hummel *et al*, 2000). We could
188 partially rescue these phenotypes by expressing *Sas-4* ubiquitously (Fig.1M and Sup. Fig. 1J
189 and L). Taken together, these results indicate that *Sas-4* mutant and downregulation conditions
190 lead to mutant phenotypes in the nervous system, characterized by incomplete penetrance
191 and variable expressivity. These phenotypes appear to be at least partially cell-autonomous,

192 as Sas-4 downregulation only in motor and sensory neurons results in axonal misrouting
193 errors.
194
195 ***Sas-4* mutant conditions disrupt muscle development**
196 Since the phenotypes induced by RNAi expression exclusively in neurons did not fully replicate
197 the strength of the motor axon defects observed in *Sas-4* embryos, we next decided to
198 investigate the muscle phenotypes in *Sas-4* mutants. Muscles play a critical role in guiding
199 motor neurons by providing chemical and physical cues essential for accurate axonal
200 pathfinding and target selection (Jeong, 2021). These signals ensure proper neuromuscular
201 connections, essential for coordinated movement. In *Drosophila* mutants lacking muscular
202 structures, such as *twist* (*twi*) embryos, the absence of these cues disrupts motor axon
203 trajectories (Younossi-Hartenstein & Hartenstein, 1993).
204 In stage 16 *Drosophila* embryos, each abdominal hemisegment (A2–A7) displays a consistent
205 and repeating pattern of 30 somatic muscle fibres, which can be visualized using a myosin-
206 specific antibody (Fig. 2A and C, wt). These 30 syncytial muscle fibres are innervated by two
207 motor nerves: the anterior ISN, which targets the dorsal muscles, and the posterior SN, which
208 innervates the ventral muscles (Fig. 2C, wt). We first analysed the muscle pattern of *Sas-4*
209 mutant embryos and could detect defects that ranged from misplaced to missing muscle fibres
210 (Fig. 2 B, B´). We then analysed these muscle fibre phenotypes in parallel to the axonal defects
211 and were able to correlate many of the axonal defects in *Sas-4* embryos to the location of the
212 muscle pattern disruptions (Fig. 2E'', asterisk and Sup. Fig. 2B'). In fact, 100% of *Sas-4*
213 embryos with detectable muscle mutant phenotypes also exhibited ISN axonal trajectory
214 disruptions, while 11% of embryos displayed ISN axonal misrouting without any observable
215 muscle phenotypes (n = 27). Accordingly, Sas-4 downregulation in muscle cells, using a *Mef2*
216 driver, induced muscle mutant phenotypes in 80% of embryos, with ISN defects spatially
217 correlating with muscle defects in 63% of the cases (n = 19, Fig. 2G'' asterisk). Sas-4
218 downregulation in muscle cells, using a *Mef2* driver together with a *Twist* (*Twi*) driver, induced

219 stronger, more penetrant ISN phenotypes that were dose dependent (Sup. Fig. 2E, F)
220 Consistent with these findings, downregulation of Sas-4 in pioneer neurons using the RN2
221 driver resulted in axonal misrouting phenotypes in 33% of the embryos (n = 15) and very mild
222 muscle mutant phenotypes in only 20% of the embryos (n = 10). Collectively, these findings
223 suggest that axonal misrouting phenotypes arise from two distinct contributions: an
224 autonomous component originating from their own CL and a non-autonomous one driven by
225 CL-affected muscle cells (Fig. 2C, *Sas-4*).
226

227 ***Sas-6* mutants have axonal guidance and muscle developmental defects**

228 Centrosome assembly depends on a small set of conserved proteins, the absence of any of
229 which results in centrosome loss; *Sas-4* and *Sas-6* are key components of this process
230 (Gartenmann *et al*, 2020). To rule out the possibility that the observed axonal and muscle
231 defects were specifically due to mutations in *Sas-4*, we began by analysing the viability of *Sas-*
232 *6* LOF mutants during the embryonic, larval, and adult stages. We used a CRISPR-Cas9
233 generated *Sas-6* induced deletion mutant, *Sas-6*$^{\Delta b}$ (Z. Novak and J. Raff, unpublished). We
234 successfully raised *Sas-6* adults (Fig. 3A), which, like *Sas-4* adults, died within 24-36 hours
235 (Fig. 1A). To corroborate that this *Sas-6* allele induced CL in embryos, we counted the number
236 of centrosomes in *Sas-6*$^{\Delta b}$ embryos and observed a reduction at stage 16 (Fig. 3B). Like *Sas-*
237 *4* mutants, 33.3% of *Sas-6*$^{\Delta b}$ and *Sas-6*$^{\Delta b}$*/Def* embryos reached embryonic stage 16,
238 corresponding to all *Sas-6*$^{\Delta b}$ homozygous and *Sas-6*$^{\Delta b}$*/Def* embryos. We only detected 11.7%
239 (n=571) of *Sas-6*$^{\Delta b}$ and 16.8% (n=486) of *Sas-6*$^{\Delta b}$*/Def* homozygous L1 larvae 36h after egg
240 laying (AEL) (Fig. 3C), corresponding to 35% of all *Sas-6* homozygous individuals and 50% of
241 *Sas-6*$^{\Delta b}$*/Def* individuals. This proportion was maintained through the wandering L3, pupal, and
242 adult stages, suggesting that, like in *Sas-4* mutants, centrosomes seem not to be essential for
243 larval and pupal development once the embryonic stages are completed.
244 We then investigated whether *Sas-6* embryos exhibited mutant axonal guidance and muscle
245 phenotypes. We observed ISN axonal misrouting in *Sas-6*$^{\Delta b}$ and *Sas-6*$^{\Delta b}$*/Def* embryos (Fig.

246 3D, F), with a penetrance of 59.1% (n=22) for *Sas-6*$^{\Delta b}$ and 54.1% (n=24) for *Sas-6*$^{\Delta b}$*/Def*,
247 similar to what we observed in *Sas-4* mutant conditions. The severity of the defects was also
248 like *Sas-4* mutant conditions, with axonal misrouting (Fig. 3F'', asterisks) and synapse (Fig.
249 F'', arrowhead) phenotypes. In most cases, the ISN axonal misrouting also correlated with
250 muscle phenotypes (Fig. 3E'' and F'', asterisks). Altogether, these findings support the role of
251 centrosomes in regulating axon guidance of motor neurons.
252
253 **Pioneer neurons have centrosomes localizing to the sites of axon outgrowth**
254 In *Drosophila*, the aCC and RP2 motor neurons are pioneer neurons which influence growth
255 of the ISN (Sánchez-Soriano & Prokop, 2005) (Fig. 4 A). Pioneer neurons extend growth cones
256 that navigate a future fibre tract, and must interpret the full complexity of environmental cues
257 to define the path of the nerve (Harrison, 1910; Jacobs & Goodman, 1989). Therefore, we
258 investigated whether centrosomes could be detected in the soma of these neurons in stage
259 12-13 when they are starting to extend their axons. We used an antibody against Pericentrin-
260 like protein (Plp, CP309) to detect the centrosome and we showed that this colocalized with
261 Asl in most cases (Sup. Fig. 3) making it a good tool to detect centrosomes in these cells. We
262 found that centrosomes were present in the soma of both aCC (Fig. 4 B and C) and RP2 motor
263 neurons (Fig. 4 D). Specifically, in the case of the aCC, a centrosome was observed in the
264 quadrant where the axon exit point is first detected in 72% of the cases (Fig. 4B n=75).
265 Additionally, we did not detect centrosomes in the quadrant opposite the axon exit point (Fig.
266 4B n=75). In *Sas-4* mutants, centrosomes were largely undetected in both aCC/pCC neurons
267 and RP2 neurons. (Fig. 4 E, F). At these stages, the aCC and pCC neurons are very close
268 together, making it difficult to differentiate between the somas of the two neurons. Therefore,
269 we quantified the number of centrosomes in aCC+pCC and RP2 neurons in both control and
270 *Sas-4* mutant embryos. In control embryos, we observed around 2.53 centrosomes per pair
271 of aCC and pCC neurons, while in *Sas-4* mutant, this number was significantly reduced to
272 0.81 (Fig. 4G n=76). Similarly, for RP2 neurons, control embryos exhibited 0.81 centrosomes
273 per RP2 neuron, whereas *Sas-4* embryos showed a reduction to 0.26 (Fig. 4G n=76). This

274 significant decrease in the number of centrosomes further supports the critical role of Sas-4
275 in centriole formation in pioneer neurons of the ventral nerve cord (VNC) during *Drosophila*
276 embryogenesis.
277
278 **Pioneer motor neurons have active centrosomes**
279 After revealing that ISN pioneers have centrosomes, we were interested in knowing if these
280 could be active MTOCs. To determine if the centriole could organize a functional centrosome
281 and serve as a major site of neuronal microtubule nucleation in aCC and RP2 neurons, we
282 analysed the localization of acetylated-tubulin (ace-tub) and γ-tubulin (γ-tub). MTs are
283 nucleated and anchored by the microtubule nucleator γ-tub, which is embedded within the
284 pericentriolar material (PCM) of the centrosome (Lin *et al*, 2015). In both neurons we could
285 see stable acetylated MTs extending from the centrosomes (Fig. 5A and B, arrowheads) and
286 these colocalized with γ-tub (Fig. 5C and D, arrowheads). We quantified the number of
287 centrioles colocalizing with γ-tub (Fig. 5E) and could detect co-localization in 50% of the cases,
288 meaning that there are centrioles in these neurons which are not active as MTOCs at these
289 stages (Fig. 5C'' asterisk). In conclusion, these results suggest that at least some microtubule
290 organization in pioneer neurons of the VNC is dependent on the centrosome.
291 To determine whether centrosomes function as active microtubule-organizing centres
292 (MTOCs) in these neurons, we tested their ability to nucleate microtubules *in vivo* using two
293 complementary approaches. First, we performed time-lapse imaging of EB1-GFP in aCC
294 neurons to visualize microtubule dynamics (Movie 1 and Fig. 5J). Second, we depolymerized
295 microtubules and monitored their regrowth from the centrosome (Fig. 5F–I) (Brodu *et al*, 2010).
296 Live imaging of aCC neurons expressing EB1-GFP and Asl-Tomato revealed EB1 comets
297 emerging from the centrosome and moving toward the cell periphery, providing direct evidence
298 of microtubule nucleation from neuronal centrosomes (Movie 1 and Fig. 5J). To strengthen this
299 observation, we performed a microtubule depolymerization/polymerization assay, which
300 unequivocally demonstrated that microtubule regrowth initiates at the centrosome following

301 depolymerization (Fig. 5F–I). This confirms that centrosomes act as active microtubule-
302 organizing centers in these neurons. Together, these findings establish that neuronal
303 centrosomes are functionally active during early axonal development.
304
305 **PNS neurons maintain active centrosomes**
306 In *Drosophila* embryos, the dorsal cluster neurons project their axons in a highly organized
307 manner to form the sensory axonal tracts (Ghysen *et al*, 1986). During development, the axons
308 of these neurons extend dorsally and medially, connecting with their target regions and
309 fasciculating with the intersegmental nerve (ISN) to form a bundled tract for efficient sensory
310 signal routing (Hartenstein, 1988). Sensory neurons in *Drosophila* embryos are known to have
311 centrioles. These centrioles are crucial for forming basal bodies in ciliated cells, including type-
312 I sensory neurons, which are essential for the development of cilia (Jana *et al*, 2016). Since
313 we detected axonal guidance phenotypes in the axons extending from the dorsal cluster, we
314 tested for the presence of centrioles in dorsal cluster sensory neurons (Fig. 6A). We detected
315 centrioles in the soma of most of these neurons and quantified the number of centriole-positive
316 ddaC neurons (Fig. 6A", B, and C', arrowhead), finding centrioles in 81.4% of the total (Fig.
317 6B, n=43). Importantly, we also detected centrioles in dorsal bipolar neuron (dbp, also known
318 as dbd), the proposed pioneer neuron of the dorsal cluster (Fig. 6A" and C', arrow) (Martin *et*
319 *al*, 2008; Merritt & Whitington, 1995). In *Sas-4* embryos, the presence of centrioles in the
320 dorsal cluster neurons was significantly lower (Fig. 6D). In many embryos, we could not detect
321 any centrioles in the soma of the dorsal cluster neurons (Fig. 6E).
322 Based on our findings in the CNS and PNS, we decided to quantify the total number of
323 centrosomes in *Sas-4* embryos and compare them to controls. To do so, we selected equal
324 segmental areas spanning the dorsal cluster and the lateral chordotonal organs (lch) and
325 counted the total number of centrioles in stage 16 control embryos, *Sas-4* homozygous
326 embryos displaying mutant PNS phenotypes, *Sas-4* homozygous embryos with no apparent
327 mutant phenotype and *Sas-4* mutants rescued by ubiquitous Sas-4 expression (Fig. 6F). We
328 observed that *Sas-4* mutants had approximately one-third of the centrioles found in the control

329 group. Embryos without defects had significantly higher centrosome numbers compared to
330 those with mutant phenotypes. Additionally, ubiquitous expression of Sas-4 in *Sas-4* mutant
331 embryos could increase centriole numbers to levels like the control (Fig.6F). These results
332 confirm that *Sas-4* embryos gradually lose their centrioles during embryonic development. We
333 also found a correlation between axonal guidance phenotypes and the numbers of centrioles
334 per embryo (Fig. 6F).
335 To assess whether sensory neuron centrosomes are associated with MT nucleation
336 machinery, we analysed their colocalization with α-tubulin and γ-tubulin. We found that
337 sensory neuron centrosomes consistently colocalise with both markers (Fig. 6 G and H),
338 indicating the presence of structural microtubules and nucleation components at the
339 centrosome. This suggests that sensory neuron centrosomes, like motor neuron centrosomes,
340 are active during early stages of axon development.
341
342 **Centrosome loss induces motor axon fibre tortuosity**
343 Axonal tortuosity (wiggliness) is a measure of the irregularities or abnormalities in the
344 morphological structure of axons which can be associated with neurodegeneration (Bando *et*
345 *al*, 2015). When axons are "wiggly," it suggests that they are not following their usual straight
346 or organized paths, possibly due to changes in axonal cytoskeletal structure or cell-adhesion,
347 but not much is known about what triggers axonal wiggliness. Qualitative examination of
348 confocal projections showed that aCC and RP2 axons are straighter in controls than in *Sas-4*
349 mutants, revealing the tortuosity of these axons (Fig. 7 A-E, asterisks). Apart from the
350 previously characterised phenotypes such as axonal crossings (Fig. 7 B, arrowhead) and
351 misrouting, we could observe axonal wiggliness at the CNS exit points of *Sas-4* motor neurons
352 (Fig. 7 B', D and E, asterisks). Since we were interested in determining the proportion of wiggly
353 axons in the *Sas- 4* mutant and *Sas-4 RNAi* embryos, we quantified this for the aCC and RP2
354 neurons (Fig. 7 G). In *Sas-4* mutants we could detect an average of 23% aCC and 30% RP2
355 wiggly axons per total number of aCC and RP2 axons, which was significantly different from
356 the proportion of wiggly axons in the controls (6% wiggly aCC and 8% wiggly RP2 axons). The

357 same was observed for the Sas-4 downregulation in aCC, pCC and RP2 neurons (24% aCC
358 and 25% RP2 wiggly axons per total number of aCC and RP2 axons). We also quantified
359 axonal wiggliness via the ratio of Path Length in 2D (PL2D) normalized to Euclidean Distance
360 in 2D (PL2D/ED2D) for each aCC and RP2 axonal path (Arshadi *et al*, 2021). We could detect
361 significant differences between control and *Sas-4* mutant conditions (Fig. 7H). It was
362 previously shown increased JNK activity, can result in axonal wiggliness (Karkali *et al*, 2023).
363 However, when we checked JNK signalling, we could not detect any increase in JNK activity
364 in *Sas-4* neurons (Supl. Fig. 4). In conclusion, although CL does not completely inhibit axonal
365 extension, it induces significant morphological alterations (Fig. 7F), emphasising the critical
366 role of the centrosome in axonal growth.
367

368 **Discussion**

369 With this work we provide evidence that the centrosome plays a role in axonal extension,
370 navigation, and muscle development *in vivo*. Previous studies have shown that *Sas-4* and
371 *Sas-6* mutant flies can reach adulthood (Basto *et al.*, 2006; Fatalska *et al.*, 2021; Peel *et al.*,
372 2007), which initially seems incompatible with an important role for the centrosome during
373 embryonic development. However, we found that *Sas-4* and *Sas-6* homozygous null
374 conditions result in 50% of embryonic lethality.
375 *Sas-4* and *Sas-6* LOF embryos display motor axon mutant phenotypes (Fig. 1 and 3),
376 revealing that centrosomes are important for axonal extension and guidance. Additionally,
377 *Sas-4* and *Sas-6* LOF embryos exhibit muscle mutant phenotypes (Fig. 2 and 3), indicating
378 that centrosomes are also important for muscle development. Hence, the embryonic axon
379 guidance phenotypes have a dual contribution: non-autonomous one from muscle CL (Fig.
380 8A) and an autonomous one from axonal CL (Fig. 8B). Since innervation does not influence
381 the patterning, morphogenesis, maintenance, or physiological development of somatic
382 muscles in *Drosophila* embryos, the muscle defects observed are most likely due to CL in
383 muscle cells (Broadie & Bate, 1993). CL in muscle cells may impair cilia formation and nuclear

384 positioning, two processes important for muscle fibre development (Loh *et al*, 2023; Metzger
385 *et al*, 2012; Tillery *et al*, 2018). Expressing *Sas-4 RNAi* under the control of the muscle-specific
386 *Mef2-GAL4* driver induced penetrant muscle phenotypes, consistent with previous results
387 reporting the lethality of these embryos (Schnorrer *et al*, 2010). *Sas-6* embryos exhibited
388 milder muscle phenotypes than *Sas-4*, aligning with previous findings that driving *Sas-6 RNAi*
389 with a Mef2-GAL4 driver induced adult pharate lethality (Schnorrer *et al.*, 2010).
390 What could explain the variability in the consequences of CL during embryonic development?
391 Many disease-causing mutations exhibit mild or no effects in some individuals, a phenomenon
392 known as incomplete phenotype penetrance. This phenomenon is still poorly understood, but
393 recent studies in *Drosophila* suggest it is stochastic, akin to flipping a coin (Marmion *et al*,
394 2023). Although the reported study focuses on fluctuations in signalling, a similar scenario
395 could be imagined for centrosomes. In cases of centrosome duplication impairment which
396 induce CL, distribution would vary among dividing cells as development proceeds. Early
397 embryonic mitotic cycles can partly explain the differences in phenotype expressivity. The first
398 13 mitotic cycles of *Drosophila* embryos are rapid, synchronous, and occur without cell
399 division. Subsequently, three rounds of patterned mitosis occur (mitoses 14, 15, and 16).
400 Following mitosis 16, many cells enter their first G1 phase (Edgar & O'Farrell, 1990). However,
401 the nervous system lineage does not enter a terminal interphase after mitosis 16 and
402 continues to divide according to an independent program (Bodmer & Jan, 1987; Hartenstein
403 *et al*, 1987). Similarly, muscle cells, continue dividing until embryonic stage 10 (Nabel-Rosen
404 *et al*, 2005). These extra cell divisions can account for the appearance, variability and severity
405 of the phenotypes observed, as centrosome loss is exacerbated with each cell division, which
406 depletes the maternal contribution. In agreement with this, when we quantified the number of
407 centrioles present in *Sas-4* embryos displaying axonal phenotypes, we could detect a
408 decrease of about 1/3 (Fig. 6), with consistent results when we quantified the numbers of
409 centrioles in *Sas-4* aCC, pCC and RP2 neurons (Fig. 4)
410
411 **Centrosome localization in neurons and implications for axonal morphology**

412 Here we show that centrosomes are present in motor and sensory neurons and that in motor
413 neurons these centrosomes colocalize with acetylated- and γ-tubulin and are actively involved
414 in MT polymerization suggesting that they are active MTOCs in these cells (Fig. 4, 5 and 6).
415 Previous studies failed to detect colocalization of centrosomes with γ-tub in neurons (Nguyen
416 *et al.*, 2011). However, this study used Fizzy-related-GFP (Fzr-GFP) to visualise centrioles
417 and while it is clear Fzr is localized to centrioles during the cell cycle (Meghini *et al*, 2016), it
418 is not clear this localization is maintained in all fully differentiated cells (Djabrayan *et al*, 2014;
419 Huynh *et al*, 2009). This, or differences in microscopy techniques, could account for the
420 inconsistency between our results and those of others. Furthermore, centrosome localization
421 and its ability to organise MTs is more likely to be important at initial axon outgrowth stages
422 (during embryonic stages 12-13) and not once the axon has already grown (at embryonic
423 stages 15-16), which is when many of these observations were made.
424 Regarding centrosome localization and activity in neurons, we show that axonal morphology
425 in embryos with fewer centrosomes is altered. This is the first example of a morphological
426 defect in axons associated with CL in *Drosophila*, and one we consider very significant. Under
427 conditions of CL, we observe tortuous (wiggly) axons, suggesting that while CL does not
428 prevent neurons from extending axons, it does affect axonal outgrowth. CL could induce this
429 phenotype by disrupting the neuronal cytoskeleton and preventing MTs to form, be severed
430 and transported into the axons. It is known that alterations in the neuronal cytoskeleton,
431 caused by signalling deregulation such as increased JNK activity, can result in axonal
432 wiggliness (Karkali *et al.*, 2023). Also, alterations in MT dynamics in mammalian neurons have
433 been shown to decrease axonal elongation, but not its formation, giving rise to wiggly axons
434 (Rochlin *et al*, 1996). In addition, axonal tortuosity is one of the hallmarks of
435 neurodegeneration (Salvadores *et al*, 2020), which makes this phenotype a good entrance
436 point for the analysis of the progression of various neurodegenerative diseases.
437 The loss of centrosome function has been documented to disrupt various developmental
438 stages in vertebrates. In humans, CL is associated with hereditary spastic paraplegia, Bardet-

Biedl syndrome, the formation of cystic kidneys, disrupted left-right asymmetry, and microcephaly (Badano *et al*, 2005; Jaiswal & Singh, 2021). Demonstrating that CL in *Drosophila* affects the development of the nervous and muscular systems paves the way for using this model organism to further explore these human diseases.

Acknowledgments

We are grateful to M. Llimargas and J. Casanova for generously providing access to their laboratory for specific aspects of this work and for their continuous support throughout the study. We thank B. Estrada, C. González, K. Karkali, C. Klämbt, E. Martin-Blanco, J. Raff, S. Rumpf, Y. Zheng, the Bloomington Drosophila Stock Center (BDSC) and the Vienna Drosophila Stock Center (VDRC) for fly stocks and reagents. We thank K. Karkali for valuable assistance with specific quantifications and technical procedures. We extend our gratitude to Z. Novak and J. Raff for sharing two unpublished CRISPR-Cas9 made *Sas-6* fly stocks with us. Thanks also go to R. Mendez for technical assistance in all the experiments and M. Bosch for assistance and advice with confocal microscopy and software. B.G. is the recipient of a Beatriu de Pinós post-doctoral fellowship from the AGAUR (2022BP00125). This work was supported by a grant from the Spanish *Ministerio de Ciencia y Innovación* (PID2021-125860NB-I00), the Universitat de Barcelona, and a grant from the Generalitat de Catalunya (2021 SGR 1455).

Author contributions

Conceptualization: S.J.A. Methodology and Experiments: B.G., J.P., J.S.-A., J.C.-R. and S.J.A. Analysis: B.G., J.P., J.S.-A. and S.J.A. Writing: S.J.A. Reviewing and editing: S.J.A. and B.G. Supervision and Funding: S.J.A.

References

Ahmad FJ, Baas PW (1995) Microtubules released from the neuronal centrosome are transported into the axon. *Journal of Cell Science* 108 (Pt 8): 2761-2769

Anda FCd, Meletis K, Ge X, Rei D, Tsai L-H (2010) Centrosome Motility Is Essential for Initial Axon Formation in the Neocortex. *The Journal of Neuroscience* 30: 10391-10406

Anda FCd, Pollarolo G, Silva JSD, Camoletto PG, Feiguin F, Dotti CG (2005) Centrosome localization determines neuronal polarity. *Nature Cell Biology* 436: 704 - 708

Araújo SJ (2019) The Golgi Apparatus and Centriole, Functions, Interactions and Role in Disease - Centrosomes in Branching Morphogenesis. *Results Problems Cell Differ* 67: 323-336

Arshadi C, Günther U, Eddison M, Harrington KIS, Ferreira TA (2021) SNT: a unifying toolbox for quantification of neuronal anatomy. *Nature Methods* 18: 374-377

Badano JL, Teslovich TM, Katsanis N (2005) The centrosome in human genetic disease. *Nature Reviews Genetics* 6: 194-205

Bando Y, Nomura T, Bochimoto H, Murakami K, Tanaka T, Watanabe T, Yoshida S (2015) Abnormal morphology of myelin and axon pathology in murine models of multiple sclerosis. *Neurochemistry International* 81: 16-27

Basto R, Lau J, Vinogradova T, Gardiol A, Woods CG, Khodjakov A, Raff JW (2006) Flies without centrioles. *Cell* 125: 1375-1386

Bazzi H, Anderson KV (2014) Acentriolar mitosis activates a p53-dependent apoptosis pathway in the mouse embryo. *Proc Natl Acad Sci U S A* 111: E1491-1500

Bettencourt-Dias M, Glover DM (2007) Centrosome biogenesis and function: centrosomics brings new understanding. *Nat Rev Mol Cell Biol* 8: 451-463

Bodmer R, Jan YN (1987) Morphological differentiation of the embryonic peripheral neurons in Drosophila. *Roux's Arch Dev Biol*: 69-77

Broadie K, Bate M (1993) Muscle development is independent of innervation during Drosophila embryogenesis. *Development* 119: 533-543

Brodu V, Baffet AD, Droguen P-ML, Casanova J, Guichet A (2010) A developmentally regulated two-step process generates a noncentrosomal microtubule network in Drosophila tracheal cells. *Developmental Cell* 18: 790 - 801

Castellanos E, Dominguez P, Gonzalez C (2008) Centrosome Dysfunction in Drosophila Neural Stem Cells Causes Tumors that Are Not Due to Genome Instability. *Current Biology* 18: 1209-1214

Chang W, Antoku S, Östlund C, Worman HJ, Gundersen GG (2015) Linker of nucleoskeleton and cytoskeleton (LINC) complex-mediated actin-dependent nuclear positioning orients centrosomes in migrating myoblasts. *Nucleus* 6: 77-88

Cheng T, Agwu C, Shim K, Wang B, Jain S, Mahjoub MR (2023) Aberrant centrosome biogenesis disrupts nephron and collecting duct progenitor growth and fate resulting in fibrocystic kidney disease. *Development* 150

Conduit PT, Wainman A, Raff JW (2015) Centrosome function and assembly in animal cells. *Nature Reviews Molecular Cell Biology* 16: 611-624

del Castillo U, Lu W, Winding M, Lakonishok M, Gelfand VI (2015) Pavarotti/MKLP1 regulates microtubule sliding and neurite outgrowth in Drosophila neurons. *Curr Biol* 25: 200-205

Djabrayan Nareg JV, Cruz J, de Miguel C, Franch-Marro X, Casanova J (2014) Specification of Differentiated Adult Progenitors via Inhibition of Endocycle Entry in the Drosophila Trachea. *Cell Reports* 9: 859-865

Edgar BA, O'Farrell PH (1990) The three postblastoderm cell cycles of Drosophila embryogenesis are regulated in G2 by string. *Cell* 62: 469-480

Fatalska A, Stepinac E, Richter M, Kovacs L, Pietras Z, Puchinger M, Dong G, Dadlez M, Glover DM (2021) The dimeric Golgi protein Gorab binds to Sas6 as a monomer to mediate centriole duplication. *Elife* 10

Fujioka M, Lear BC, Landgraf M, Yusibova GL, Zhou J, Riley KM, Patel NH, Jaynes JB (2003) Even-skipped, acting as a repressor, regulates axonal projections in Drosophila. *Development* 130: 5385-5400

Gartenmann L, Vicente CC, Wainman A, Novak ZA, Sieber B, Richens JH, Raff JW (2020) Drosophila Sas-6, Ana2 and Sas-4 self-organise into macromolecular structures that can be used to probe centriole and centrosome assembly. *Journal of Cell Science* 133: jcs244574

Ghysen A, Dambly-Chaudière C, Aceves E, Jan L, Jan Y (1986) Sensory neurons and peripheral pathways in Drosophila embryos. *Rouxs Arch Dev Biol* 195: 281-289

523 Gogendeau D, Basto R (2010) Centrioles in flies: The exception to the rule? *Semin Cell Dev*
524 *Biol* 21: 163-173
525 Gomes ER, Jani S, Gundersen GG (2005) Nuclear Movement Regulated by Cdc42, MRCK,
526 Myosin, and Actin Flow Establishes MTOC Polarization in Migrating Cells. *Cell* 121: 451-463
527 Goundiam O, Basto R (2020) Centrosomes in disease: how the same music can sound so
528 different? *Current opinion in structural biology* 66: 74-82
529 Grzonka M, Bazzi H (2024) Mouse SAS-6 is required for centriole formation in embryos and
530 integrity in embryonic stem cells. *eLife* 13: e94694
531 Harrison RG (1910) The outgrowth of the nerve fiber as a mode of protoplasmic movement.
532 *Journal of Experimental Zoology* 9: 787-846
533 Hartenstein V (1988) Development of Drosophila larval sensory organs: spatiotemporal
534 pattern of sensory neurones, peripheral axonal pathways and sensilla differentiation.
535 *Development* 102: 869-886
536 Hartenstein V, Rudloff E, Campos-Ortega JA (1987) The pattern of proliferation of the
537 neuroblasts in the wild-type embryo of Drosophila melanogaster. *Rouxs Arch Dev Biol* 196:
538 473-485
539 Hummel T, Krukkert K, Roos J, Davis G, Klämbt C (2000) Drosophila Futsch/22C10 Is a
540 MAP1B-like Protein Required for Dendritic and Axonal Development. *Neuron* 26: 357-370
541 Huynh MA, Stegmüller J, Litterman N, Bonni A (2009) Regulation of Cdh1-APC function in
542 axon growth by Cdh1 phosphorylation. *J Neurosci* 29: 4322-4327
543 Jacobs J, Goodman C (1989) Embryonic development of axon pathways in the Drosophila
544 CNS. II. Behavior of pioneer growth cones. *The Journal of Neuroscience* 9: 2412-2422
545 Jaiswal S, Singh P (2021) Centrosome dysfunction in human diseases. *Semin Cell Dev Biol*
546 110: 113-122
547 Jana SC, Bettencourt-Dias M, Durand B, Megraw TL (2016) Drosophila melanogaster as a
548 model for basal body research. *Cilia*: 1-7
549 Jeong S (2021) Molecular Mechanisms Underlying Motor Axon Guidance in Drosophila.
550 *Molecules and Cells* 44: 549-556
551 Karkali K, Vernon SW, Baines RA, Panayotou G, Martín-Blanco E (2023) Puckered and JNK
552 signaling in pioneer neurons coordinates the motor activity of the Drosophila embryo. *Nature*
553 *Communications* 14: 8186
554 Kopeć S (1928) On the Influence of Intermittent Starvation on the Longevity of the Imaginal
555 Stage of Drosophila Melanogaster. *Journal of Experimental Biology* 5: 204-211
556 Kushner EJ, Ferro LS, Liu J-Y, Durrant JR, Rogers SL, Dudley AC, Bautch VL (2014) Excess
557 centrosomes disrupt endothelial cell migration via centrosome scattering. *J Cell Biol* 206:
558 257-272
559 Leask A, Obrietan K, Stearns T (1997) Synaptically coupled central nervous system neurons
560 lack centrosomal γ-tubulin. *Neuroscience Letters* 229: 17-20
561 Leidel S, Gönczy P (2003) SAS-4 is essential for centrosome duplication in C elegans and is
562 recruited to daughter centrioles once per cell cycle. *Dev Cell* 4: 431-439
563 Lin T-c, Neuner A, Schiebel E (2015) Targeting of γ-tubulin complexes to microtubule
564 organizing centers: conservation and divergence. *Trends in Cell Biology* 25: 296-307
565 Lindhout FW, Portegies S, Kooistra R, Herstel LJ, Stucchi R, Hummel JJA, Scheefhals N,
566 Katrukha EA, Altelaar M, MacGillavry HD *et al* (2021) Centrosome-mediated microtubule
567 remodeling during axon formation in human iPSC-derived neurons. *The EMBO Journal* 40:
568 e106798
569 Loh M, Bernard F, Guichet A (2023) Kinesin-1 promotes centrosome clustering and nuclear
570 migration in the Drosophila oocyte. *Development* 150
571 Marmion RA, Simpkins AG, Barrett LA, Denberg DW, Zusman S, Schottenfeld-Roames J,
572 Schüpbach T, Shvartsman SY (2023) Stochastic phenotypes in RAS-dependent
573 developmental diseases. *Current Biology* 33: 807-816.e804
574 Marthiens V, Rujano MA, Pennetier C, Tessier S, Paul-Gilloteaux P, Basto R (2013)
575 Centrosome amplification causes microcephaly. *Nat Cell Biol* 15: 731-740

Martin V, Mrkusich E, Steinel MC, Rice J, Merritt DJ, Whitington PM (2008) The L1-type cell adhesion molecule Neuroglian is necessary for maintenance of sensory axon advance in the Drosophila embryo. *Neural Dev* 3: 10

Meghini F, Martins T, Tait X, Fujimitsu K, Yamano H, Glover DM, Kimata Y (2016) Targeting of Fzr/Cdh1 for timely activation of the APC/C at the centrosome during mitotic exit. *Nat Commun* 7: 12607

Meka DP, Kobler O, Hong S, Friedrich CM, Wuesthoff S, Henis M, Schwanke B, Krisp C, Schmuelling N, Rueter R *et al* (2022) Centrosome-dependent microtubule modifications set the conditions for axon formation. *Cell Reports* 39: 110686

Merritt DJ, Whitington PM (1995) Central projections of sensory neurons in the Drosophila embryo correlate with sensory modality, soma position, and proneural gene function. *J Neurosci* 15: 1755-1767

Metzger T, Gache V, Xu M, Cadot B, Folker ES, Richardson BE, Gomes ER, Baylies MK (2012) MAP and kinesin-dependent nuclear positioning is required for skeletal muscle function. *Nature* 484: 120-124

Meyer-Gerards C, Bazzi H (2025) Developmental and tissue-specific roles of mammalian centrosomes. *FEBS J* 292: 709-726

Nabel-Rosen H, Toledano-Katchalski H, Volohonsky G, Volk T (2005) Cell Divisions in the Drosophila Embryonic Mesoderm Are Repressed via Posttranscriptional Regulation of string/cdc25 by HOW. *Current Biology* 15: 295-302

Nguyen MM, Stone MC, Rolls MM (2011) Microtubules are organized independently of the centrosome in Drosophila neurons. *Neural Development* 6: 38

Pearl R, Parker SL (1921) Experimental Studies on the Duration of Life. I. Introductory Discussion of the Duration of Life in Drosophila. *Am Nat* 55: 481-509

Peel N, Stevens NR, Basto R, Raff JW (2007) Overexpressing Centriole-Replication Proteins In Vivo Induces Centriole Overduplication and De Novo Formation. *Current Biology* 17: 834-843

Poulton John S, Cuningham John C, Peifer M (2014) Acentrosomal Drosophila Epithelial Cells Exhibit Abnormal Cell Division, Leading to Cell Death and Compensatory Proliferation. *Developmental Cell* 30: 731-745

Poulton JS, Cuningham JC, Peifer M (2017) Centrosome and spindle assembly checkpoint loss leads to neural apoptosis and reduced brain size. *Journal of Cell Biology* 216: 1255-1265

Ricolo D, Castro-Ribera J, Araújo SJ (2021) Cytoskeletal players in single-cell branching morphogenesis. *Developmental Biology* 477: 22-34

Ricolo D, Deligiannaki M, Casanova J, Araújo SJ (2016) Centrosome Amplification Increases Single-Cell Branching in Post-mitotic Cells. *Curr Biol* 26: 2805-2813

Rochlin MW, Wickline KM, Bridgman PC (1996) Microtubule Stability Decreases Axon Elongation but Not Axoplasm Production. *The Journal of Neuroscience* 16: 3236-3246

Salvadores N, Gerónimo-Olvera C, Court FA (2020) Axonal Degeneration in AD: The Contribution of Aβ and Tau. *Front Aging Neurosci* 12: 581767

Sanchez-Huertas C, Freixo F, Viais R, Lacasa C, Soriano E, Luders J (2016) Non-centrosomal nucleation mediated by augmin organizes microtubules in post-mitotic neurons and controls axonal microtubule polarity. *Nat Commun* 7: 12187

Sánchez-Soriano N, Prokop A (2005) The influence of pioneer neurons on a growing motor nerve in Drosophila requires the neural cell adhesion molecule homolog FasciclinII. *J Neurosci* 25: 78-87

Schnorrer F, Schönbauer C, Langer CCH, Dietzl G, Novatchkova M, Schernhuber K, Fellner M, Azaryan A, Radolf M, Stark A *et al* (2010) Systematic genetic analysis of muscle morphogenesis and function in Drosophila. *Nature* 464: 287-291

Stevens NR, Raposo AASF, Basto R, Johnston DS, Raff JW (2007) From Stem Cell to Embryo without Centrioles. 17: 1498-1503

Stiess M, Maghelli N, Kapitein LC, Gomis-Rüth S, Wilsch-Bräuninger M, Hoogenraad CC, Tolić-Nørrelykke IM, Bradke F (2010) Axon extension occurs independently of centrosomal microtubule nucleation. *Science* 327: 704-707

631 Tillery MML, Blake-Hedges C, Zheng Y, Buchwalter RA, Megraw TL (2018) Centrosomal and
632 Non-Centrosomal Microtubule-Organizing Centers (MTOCs) in Drosophila melanogaster.
633 *Cells* 7
634 Varmark H, Llamazares S, Rebollo E, Lange B, Reina J, Schwarz H, Gonzalez C (2007)
635 Asterless is a centriolar protein required for centrosome function and embryo development in
636 Drosophila. *Curr Biol* 17: 1735-1745
637 Vinopal S, Dupraz S, Alfadil E, Pietralla T, Bendre S, Stiess M, Falk S, Ortega GC, Maghelli
638 N, Tolić IM *et al* (2023) Centrosomal microtubule nucleation regulates radial migration of
639 projection neurons independently of polarization in the developing brain. *Neuron* 111: 1241-
640 1263.e1216
641 Younossi-Hartenstein A, Hartenstein V (1993) The role of the tracheae and musculature
642 during pathfinding of Drosophila embryonic sensory axons. *Dev Biol* 158: 430-447
643 Yu W, Centonze VE, Ahmad FJ, Baas PW (1993) Microtubule nucleation and release from
644 the neuronal centrosome. *The Journal of cell biology* 122: 349-359
645

646 **Figure legends**

647

648 **Fig. 1 – *Sas-4* loss of function induces axonal misrouting defects.**

649 (A) *Sas-4* homozygous adult fly at 6h after eclosion. (B) Graphical representation of the
650 percentage of *Sas-4* (n=407) and *Sas-4/Def* (n=337) surviving individuals at different life cycle
651 stages. Homozygous flies that survive to adult stages die after 24-36 hours. (C) Highlight of
652 the three main FasII positive nerves over a microscope image of two embryonic lateral
653 segments. (D-G) Details of three segments from stage 16 embryos stained with anti-FasII
654 antibody; scale bar 10 µm. (D'-G') Confocal lateral views of stage 16 embryos stained with
655 anti-FasII antibody; scale bar 50 µm. (H) Penetrance and expressivity of the ISN mutant
656 phenotypes in different *Sas-4* mutant conditions; control is *w* (n=35); *Sas-4*^{s2214} (n=53); *Sas-*
657 *4*^{s2214}*/Df* (n=25); *RN2Gal4xUASSas-4RNAi* (n=15); *UbqSas-4GFP;Sas-4/Df* (n=28). (I-L)
658 Details of three segments from stage 16 embryos stained with anti-Futsch antibody; scale bar
659 5 µm (I'-L') Confocal lateral views of stage 16 embryos stained with anti-Futsch antibody; scale
660 bar 50 µm. (H) Penetrance and expressivity of the sensory axon mutant phenotypes in
661 different *Sas-4* mutant conditions; control is *Sas-4/+* (n=20); *Sas-4*^{s2214} (n=20); *Sas-4*^{s2214}*/Df*
662 (n=20); *P0163Gal4xUASSas-4RNAi* (n=20); *UbqSas-4GFP;Sas-4/Df* (n=20).

663

664 **Fig. 2 - *Sas-4* loss of function induces muscle defects.**

665 (A,B) Stage 16 embryos stained with an antibody against myosin to mark the embryonic
666 muscle structure in green. (A-A') Control embryo and (B-B') *Sas-4* mutant embryo. (C)
667 Schematic representation of the motor axon muscle innervation pattern of a control (*w*) and
668 *Sas-4* mutant embryo. TN, transverse nerve; ISN, intersegmental nerve, and SN, segmental
669 nerve. (D-H) Confocal projections of four segments from stage 16 embryos of different mutant
670 conditions stained with anti-myosin (green and D') and anti-FasII (magenta and D'') antibodies;
671 scale bar 10 µm. (D''-H'') composite images with the two channels (anti-myosin in green and
672 anti-FasII in magenta). (D'''-H''') Myosin-stained muscle single-stacks. Scale bar 10 µm. (I)
673 Penetrance and expressivity of the ISN mutant phenotypes in different *Sas-4* mutant
674 conditions; control is *Sas-4/+* (n=27); *Sas-4*^{s2214} (n=27); *Sas-4*^{s2214}*/Df* (n=25);
675 *Mef2Gal4xUASSas-4RNAi* (n=19); *RN2Gal4xUASSas-4RNAi* (n=15). (J) Penetrance and
676 expressivity of the muscle mutant phenotypes in different *Sas-4* mutant conditions; control is
677 *w* (n=16); *Sas-4*^{s2214} (n=16); *Sas-4*^{s2214}*/Df* (n=10); *Mef2Gal4xUASSas-4RNAi* (n=10);
678 *RN2Gal4xUASSas-4RNAi* (n=16).
679
680 **Fig. 3 - *Sas-6* loss of function induces axonal misrouting and muscle defects.**
681 (A) *Sas-6* homozygous adult fly at 6h after eclosion. (B) Quantification of the number of
682 centrosomes per stage 16 embryonic segmental area in Control, *Sas-6*$^{\Delta b}$/+ embryos, (mean
683 165.9 ± 26.4, n=10) and *Sas-6*$^{\Delta b}$ embryos displaying PNS mutant phenotypes (mean 53.2 ±
684 21.9, n=15); unpaired t-test with Welch's correction p<0.0001. (C) Graphical representation of
685 the percentage of *Sas-6*$^{\Delta b}$/*Sas-6*$^{\Delta b}$ (n=571) and *Sas-6*$^{\Delta b}$/Def (n=486) surviving individuals at
686 different life-cycle stages. (D) Penetrance and expressivity of the ISN mutant embryonic
687 phenotypes in *Sas-6*$^{\Delta b}$ and *Sas-6*$^{\Delta b}$/Def embryos; controls are heterozygous *Sas-6*$^{\Delta b}$/+ (n=17);
688 mutants are *Sas-6*$^{\Delta b/\Delta b}$ (n=22) and *Sas-6*$^{\Delta b}$/Def (n=24). (E, F) Confocal projections of four
689 segments from stage 16 embryos of control and *Sas-6*$^{\Delta b}$/Def mutants stained with anti-myosin
690 (magenta and E', F') and anti-FasII (green and E, F) antibodies. (E''-F'') Composite projections
691 with the two channels; scale bar is 10 µm. (E'''-F''') Composite projections of the two channels
692 showing the whole embryo; scale bar is 50µm.

693

694 **Fig. 4 - Pioneer neurons have centrosomes localizing to the sites of axon outgrowth**

695 (A) Confocal image showing 3 segments of the embryonic Ventral Nerve Cord (VNC) midline
696 marked with an antibody against FasII and GFP driven by the RN2 driver marking the aCC,
697 pCC and RP2 in green. (B) Confocal section showing an aCC neuron and its centriole at the
698 axonal exit point, marked with an antibody against Plp (CP309); quantification of centrioles
699 present in different aCC quadrants and the percentage of aCC with centrioles present at the
700 axonal exit point (72%, n=75). (C, D) Plp (CP309) marking all centrosomes and the neuronal
701 body drawn from the channel marking the neuron (C', D'). (C'') aCC+pCC and RP2 (D'')
702 marked in green and Plp (CP309) in magenta. Scale bar is 5µm. (G) Quantification of centriole
703 numbers in control and *Sas-4* aCC+pCC and RP2 pioneer neurons; Control RP2 average 0.81
704 (n=22), control aCC+pCC average 2.53 (n=41), *Sas-4* RP2 average 0.26 (n=34) and *Sas-4*
705 aCC+pCC average 0.87 (n=38); unpaired t-test with Welch's correction control RP2 vs *Sas-4*
706 RP2 p=0.0005, control aCC+pCC vs *Sas-4* aCC+pCC p<0.0001.

707

708 **Fig. 5 – PNS neurons maintain their centrosomes**

709 (A) Dorsal cluster neurons in a stage 15 embryo marked with anti-Futsch (22C10) in magenta
710 to mark the sensory neurons and Asterless (Asl) in green to mark the centrosomes. (A')
711 Inverted channels with neurons identified and (A'') cell bodies drawn to show the centrosomes
712 within each neuron. Scale bar is 8 µm (B) Stage 16 dorsal cluster with the neurons identified
713 and ddaC marked in green with ppkGAL4 driving UASCD8GFP marking class IV dendritic
714 arborisation neurons, with centriole in cyan and Futsch in green. Scale bar is 5 µm.
715 Quantification of the number of ddaC neurons with centrosomes (81.4% n=43). (C) Control
716 and *Sas-4* (D,E) dorsal clusters marked with Futsch in magenta and Plp (CP309) in green.
717 (C', D' and E') Plp (CP309) marking all centrosomes and cell bodies drawn from the other
718 channel (C'', D'' and E''); scale bar Is 5 µm. (F) Quantification of the number of centrosomes
719 per stage 16 embryonic segmental area in Control, *Sas-4/+* embryos, (mean 179.4 ± 30.1,
720 n=25), *Sas-4* embryos displaying PNS mutant phenotypes (mean 68.2 ± 21.6, n=23), *Sas-4*

721 embryos without detectable PNS mutant phenotypes (mean 86.3 ± 23.8, n=24) and *Sas-4*
722 embryos rescued by ubiquitous expression of Sas-4 (mean 157.3 ± 51.45, n=23); unpaired t-
723 test with Welch's correction control vs *Sas-4* p<0.0001, control vs *Sas-4* no defects p<0.0001,
724 control vs *Sas-4* rescue p=0.08 and *Sas-4* vs *Sas-4* no defects p=0.009. (G) Detail of the
725 dorsal part of the dorsal cluster stained marked with Futsch (green), Plp (CP309) (magenta),
726 and alpha-tubulin (blue); arrowheads point to the colocalization of centrosomes with MTs. (H)
727 Detail of the dorsal part of the dorsal cluster stained marked with Futsch (green), Plp (CP309)
728 (magenta), and gamma-tubulin (blue); arrowheads point to the colocalization of centrosomes
729 with gamma-tubulin; scale bar is 2.5 µm.
730
731 **Fig. 6 – Pioneer motor neurons have active centrosomes**
732 (A) RN2>CD8GFP with aCC+pCC and RP2 (B) marked in green, Plp (CP309) in magenta and
733 ace-tub in blue; scale bar 5 µm. (A', B') Plp (CP309) marking all centrioles and the neuronal
734 body drawn from the channel marking the neuron (A, B). (A'', B'') Plp (CP309) marking all
735 centrioles and acetylated-tubulin antibody marking stable MTs with the neuronal body drawn
736 from the channel marking the neuron (A, B). (C) aCC+pCC and RP2 (D) marked in green, Plp
737 (CP309) in magenta and γ-tub in blue. (C', D') Plp (CP309) marking all centrosomes and the
738 neuronal body drawn from the channel marking the neuron (C, D). (C'', D'') Plp (CP309)
739 marking all centrosomes and anti-acetylated-tubulin antibody marking stable MTs with the
740 neuronal body drawn from the channel marking the neuron (C, D). (E) Quantification of the
741 total number of centrioles in aCC+pCC and RP2 neurons and quantification of the numbers of
742 these which colocalize with γ-tub (n=18). (F-I) RN2>CD8GFP with aCC+pCC marked in green,
743 Plp (CP309) in magenta and alpha-tub in blue; scale bar 5 µm. (F'-I') Plp (CP309) marking all
744 centrosomes and anti-alpha-tubulin antibody marking all MTs, with the neuronal body drawn
745 from the channel marking the neuron (F-I). (F) Control embryos, 0h at 4°C; (G) embryos
746 incubated 6h at 4°C; (H) embryos incubated 6h at 4°C and allowed to recover for 90 seconds
747 at RT; (I) embryos incubated 6h at 4°C and allowed to recover for 5 min at RT. Scale bar 5 µm.

748 (J) Frames from Movie 1 showing the localization of EB1-GFP with the centrosome (asterisks)
749 and its displacement towards the axon (arrows) in an aCC neuron; scale bar 5 μm. (K)
750 Colocalization of EB1(arrow) with the centrosome (asterisk) in a fixed aCC neuron; scale bar
751 5 μm.
752
753 **Fig. 7 - *Sas-4* loss of function induces wiggly axon phenotypes**
754 (A-E) Confocal images of stage 16 RN2GAL4, UASCD8GFP embryonic lateral segments
755 (A,B) or the ventral midline (CEF) in wt (A, C), *Sas-4* mutant background (B, D) or Sas-4 RNAi
756 downregulation (E). (A',B') axons marked with anti-FasII and (A'', B'', C, D, E) axons marked
757 with anti-GFP antibody, marking the axonal membranes. Scale bar is 10 μm in A-E. (F)
758 Schematic representation of the wiggly axon phenotypes; in *Sas-4* aCC and RP2 neurons, the
759 absence of active centrosomes gives rise to axonal tortuosity. **(**G) Quantification of the
760 proportion (wiggly/normal axons) of wiggly axons in control, *Sas-4* mutant and Sas-4 RNAi
761 downregulation for aCC and RP2 neurons; Mann-Whitney test p=0.025 in control vs *Sas-4*
762 aCC (n=8 embryos); p= 0.0026 in control vs Sas-4 RNAi aCC (n=8 embryos) and p=0.0065
763 in control vs *Sas-4* RP2 (n=8 embryos); p=0.0149 in control vs Sas-4 RNAi RP2 (n=8
764 embryos). (H) Quantification of axonal wiggliness via the ratio of Path Length in 2D (PL2D)
765 normalized to Euclidean Distance in 2D (PL2D/ED2D) for each aCC and RP2 axonal path.
766 Mann-Whitney test p=0.0002 in control (n= 33 axons) vs *Sas-4* aCC (n=36 axons); p< 0.0001
767 in control vs Sas-4 RNAi aCC (n=41 axons) and p< 0.0001 in control (n=35 axons) vs *Sas-4*
768 RP2 (n= 36 axons); p< 0.0001 in control vs Sas-4 RNAi RP2 (n= 41 axons).
769
770 **Fig. 8 – Centrosome loss affects axonal morphogenesis and muscle development**
771 Schematic representations of CL induced axonal phenotypes. CL disrupts axonal
772 morphogenesis and pathfinding through two distinct mechanisms. (A) First, in a neuron non-
773 autonomous manner, CL impairs muscle development, which in turn leads to axon guidance
774 defects. (B) Second, in a neuron-autonomous manner, CL compromises the integrity of the
775 MT cytoskeleton, resulting in defective axon pathfinding and increased axonal tortuosity.

776 Together, these effects unravel the multifaceted role of the centrosome in coordinating both
777 extrinsic and intrinsic cues essential for proper axonal development.

Fig. 1

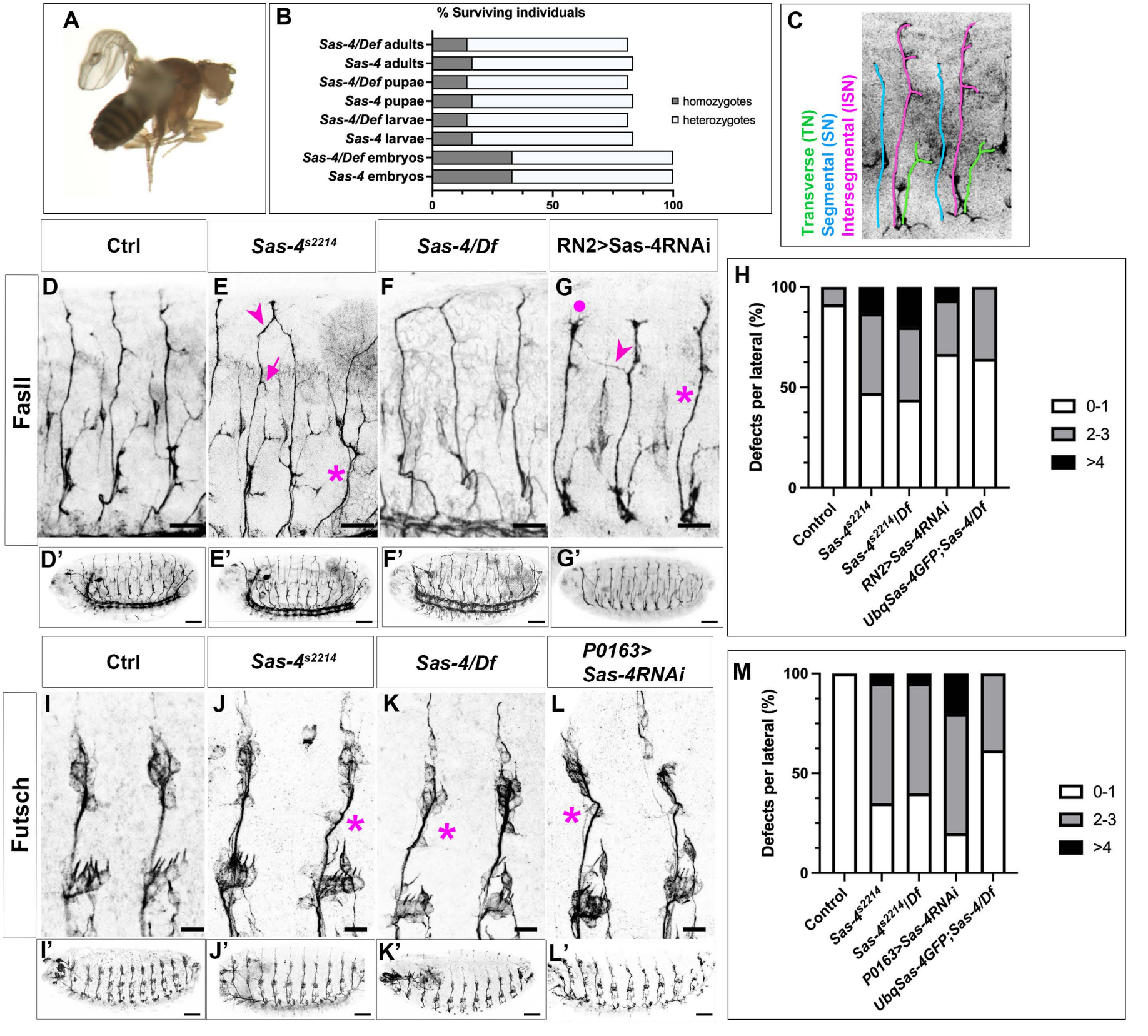
A
B
% Surviving individuals
Sas-4/Def adults
Sas-4 adults
Sas-4/Def pupae
Sas-4 pupae
Sas-4/Def larvae
Sas-4 larvae
Sas-4/Def embryos
Sas-4 embryos
homozygotes
heterozygotes
0
50
100
C
Transverse (TN)
Segmental (SN)
Intersegmental (ISN)
Ctrl
Sas-4s2214
Sas-4/Df
RN2>Sas-4RNAi
FasII
D
E
F
G
D'
E'
F'
G'
H
Defects per lateral (%)
100
50
0
Control
Sas-4s2214
Sas-4s2214/Df
RN2>Sas-4RNAi
UbqSas-4GFP;Sas-4/Df
0-1
2-3
>4
Ctrl
Sas-4s2214
Sas-4/Df
P0163>
Sas-4RNAi
Futsch
I
J
K
L
I'
J'
K'
L'
M
Defects per lateral (%)
100
50
0
Control
Sas-4s2214
Sas-4s2214/Df
P0163>Sas-4RNAi
UbqSas-4GFP;Sas-4/Df
0-1
2-3
>4

Fig 2

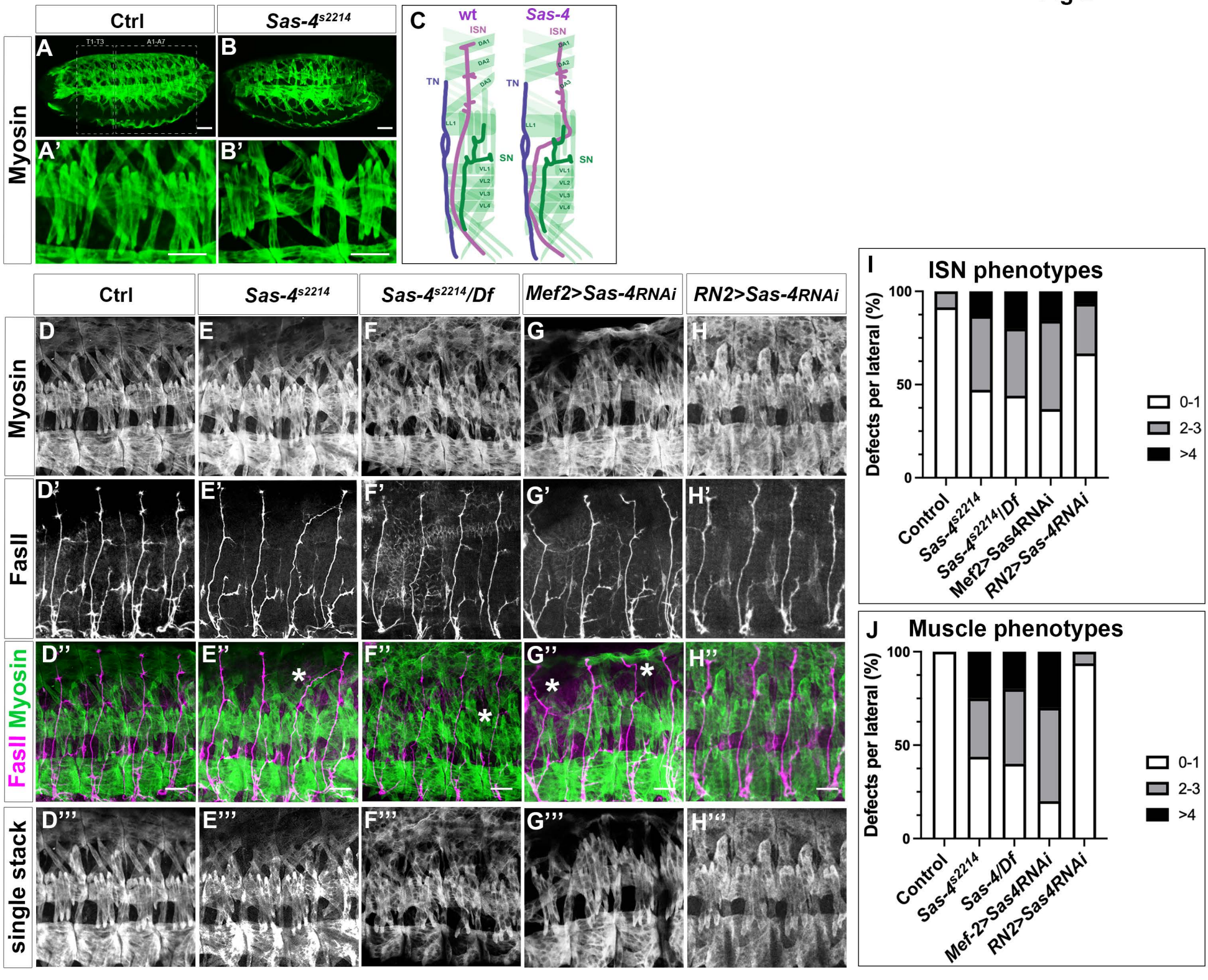
Ctrl
Sas-4s2214
Myosin
A
B
A'
B'
T1-T3
A1-A7
C
wt
Sas-4
ISN
TN
LL1
SN
DA1
DA2
DA3
VL1
VL2
VL3
VL4
Ctrl
Sas-4s2214
Sas-4s2214/Df
Mef2>Sas-4RNAi
RN2>Sas-4RNAi
Myosin
FasII
FasII Myosin
single stack
D
E
F
G
H
D'
E'
F'
G'
H'
D''
E''
F''
G''
H''
D'''
E'''
F'''
G'''
H'''
I
ISN phenotypes
Defects per lateral (%)
100
50
0
Control
Sas-4s2214
Sas-4s2214/Df
Mef2>Sas4RNAi
RN2>Sas-4RNAi
0-1
2-3
>4
J
Muscle phenotypes
Defects per lateral (%)
100
50
0
Control
Sas-4s2214
Sas-4/Df
Mef-2>Sas4RNAi
RN2>Sas4RNAi
0-1
2-3
>4

Fig. 3

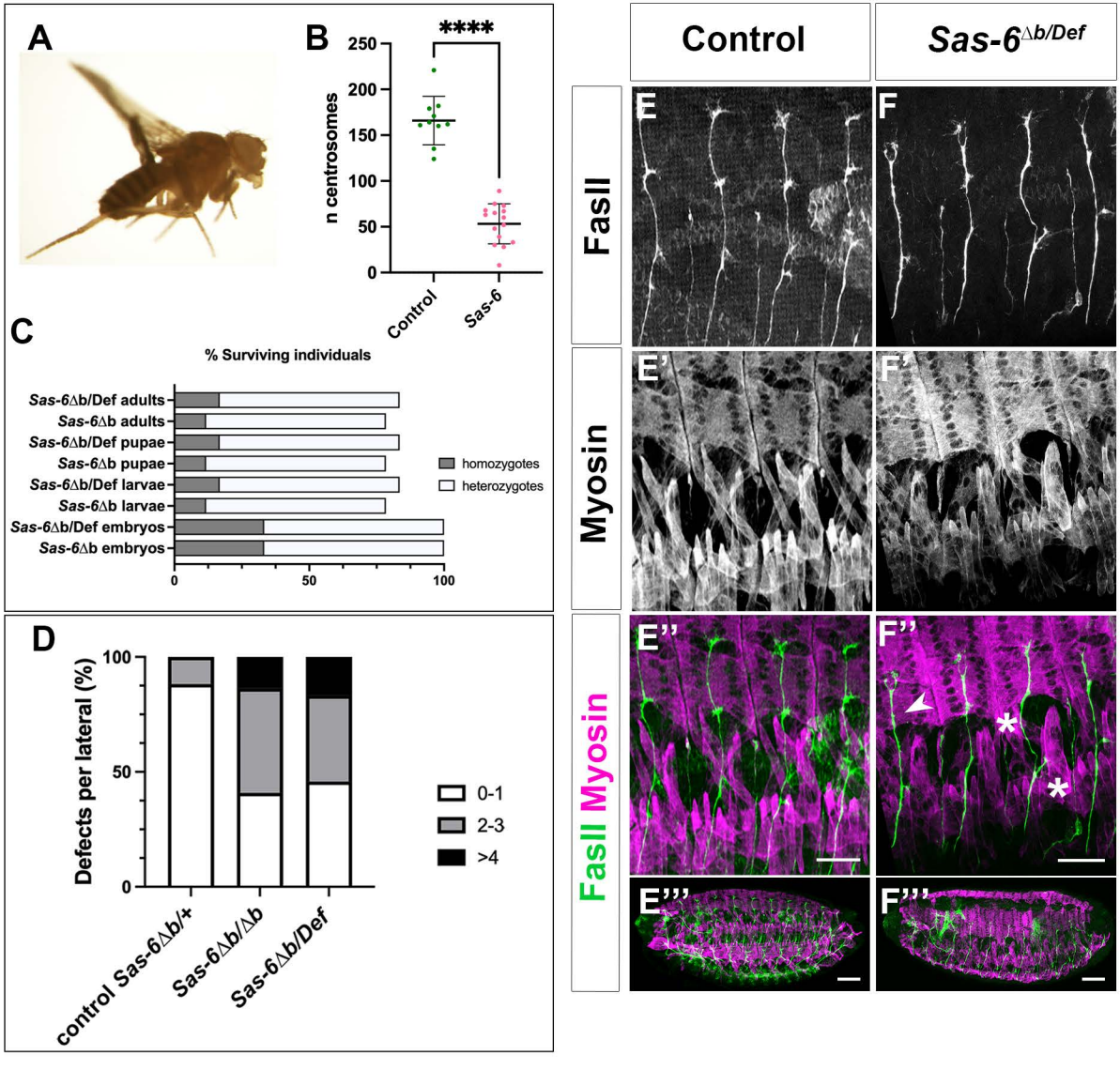
A
B
****
n centrosomes
250
200
150
100
50
0
Control
Sas-6
C
% Surviving individuals
Sas-6Δb/Def adults
Sas-6Δb adults
Sas-6Δb/Def pupae
Sas-6Δb pupae
Sas-6Δb/Def larvae
Sas-6Δb larvae
Sas-6Δb/Def embryos
Sas-6Δb embryos
homozygotes
heterozygotes
0
50
100
D
Defects per lateral (%)
100
50
0
0-1
2-3
>4
control Sas-6Δb/+
Sas-6Δb/Δb
Sas-6Δb/Def
Control
Sas-6Δb/Def
FasII
Myosin
FasII Myosin
E
F
E'
F'
E''
F''
E'''
F'''

Fig. 4

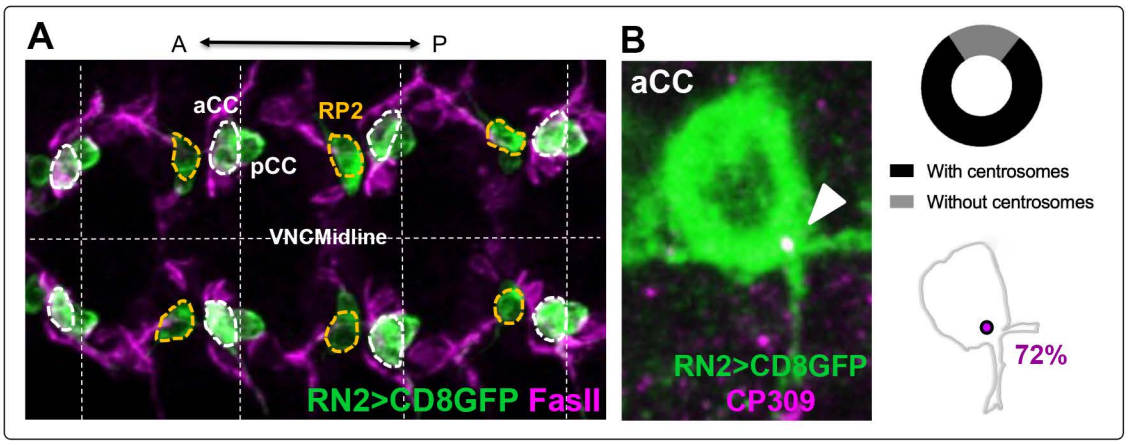
A
A
P
aCC
RP2
pCC
VNCMidline
RN2>CD8GFP FasII
B
aCC
RN2>CD8GFP
CP309
With centrosomes
Without centrosomes
72%

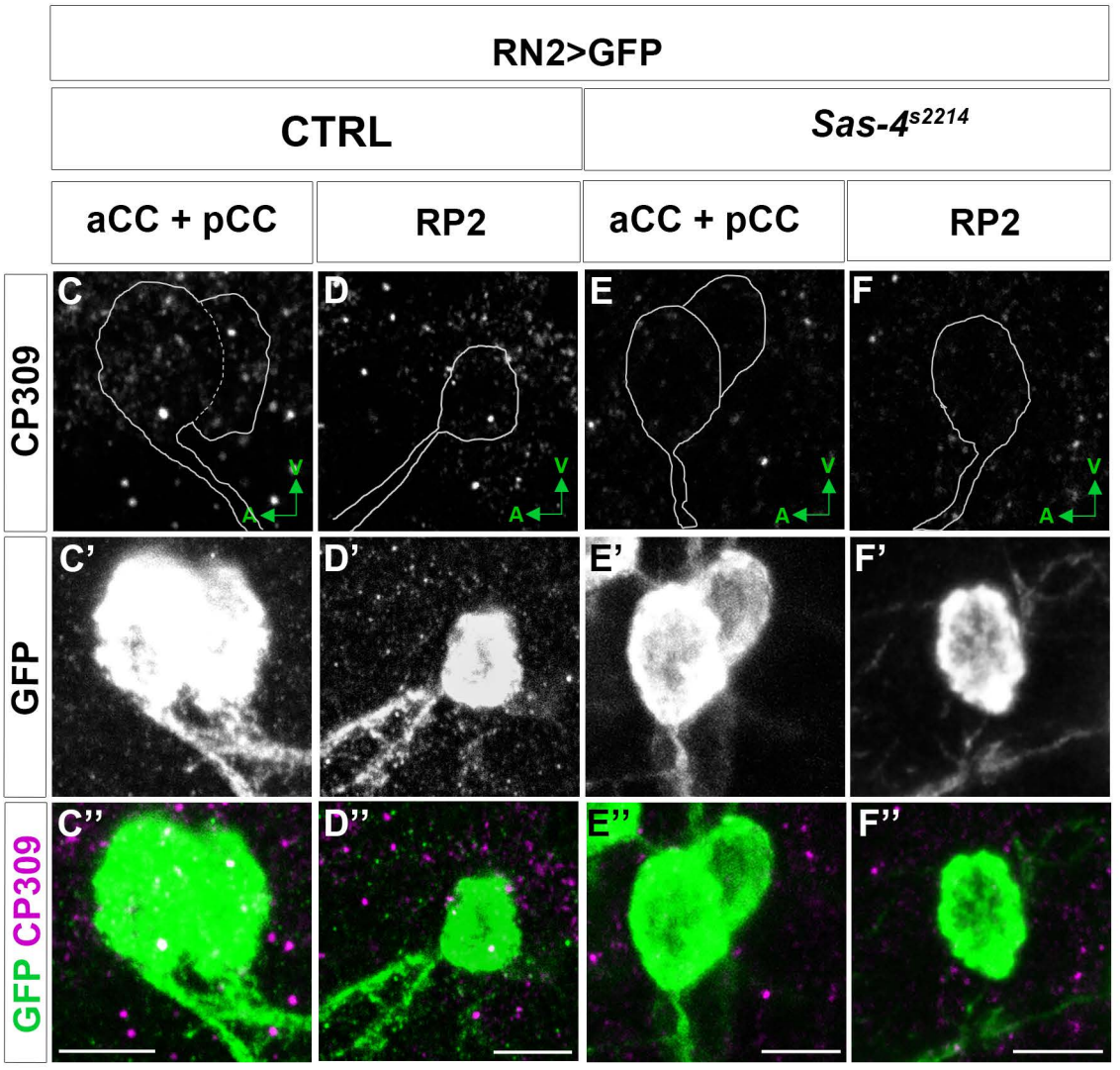
RN2>GFP
CTRL
Sas-4s2214
aCC + pCC
RP2
aCC + pCC
RP2
CP309
GFP
GFP CP309
C
D
E
F
C'
D'
E'
F'
C''
D''
E''
F''
V
A

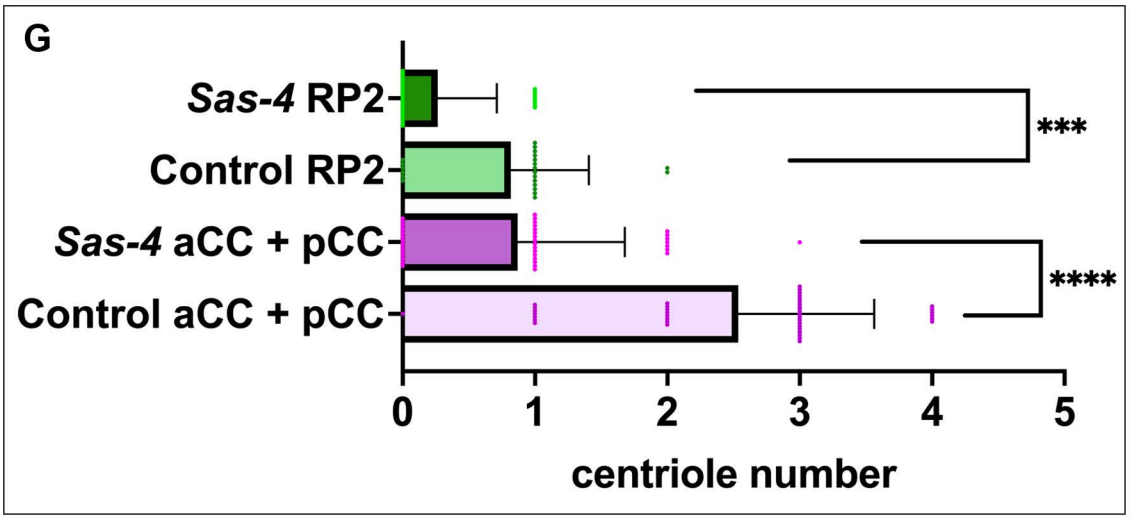
G
Sas-4 RP2
Control RP2
Sas-4 aCC + pCC
Control aCC + pCC
***
****
0
1
2
3
4
5
centriole number

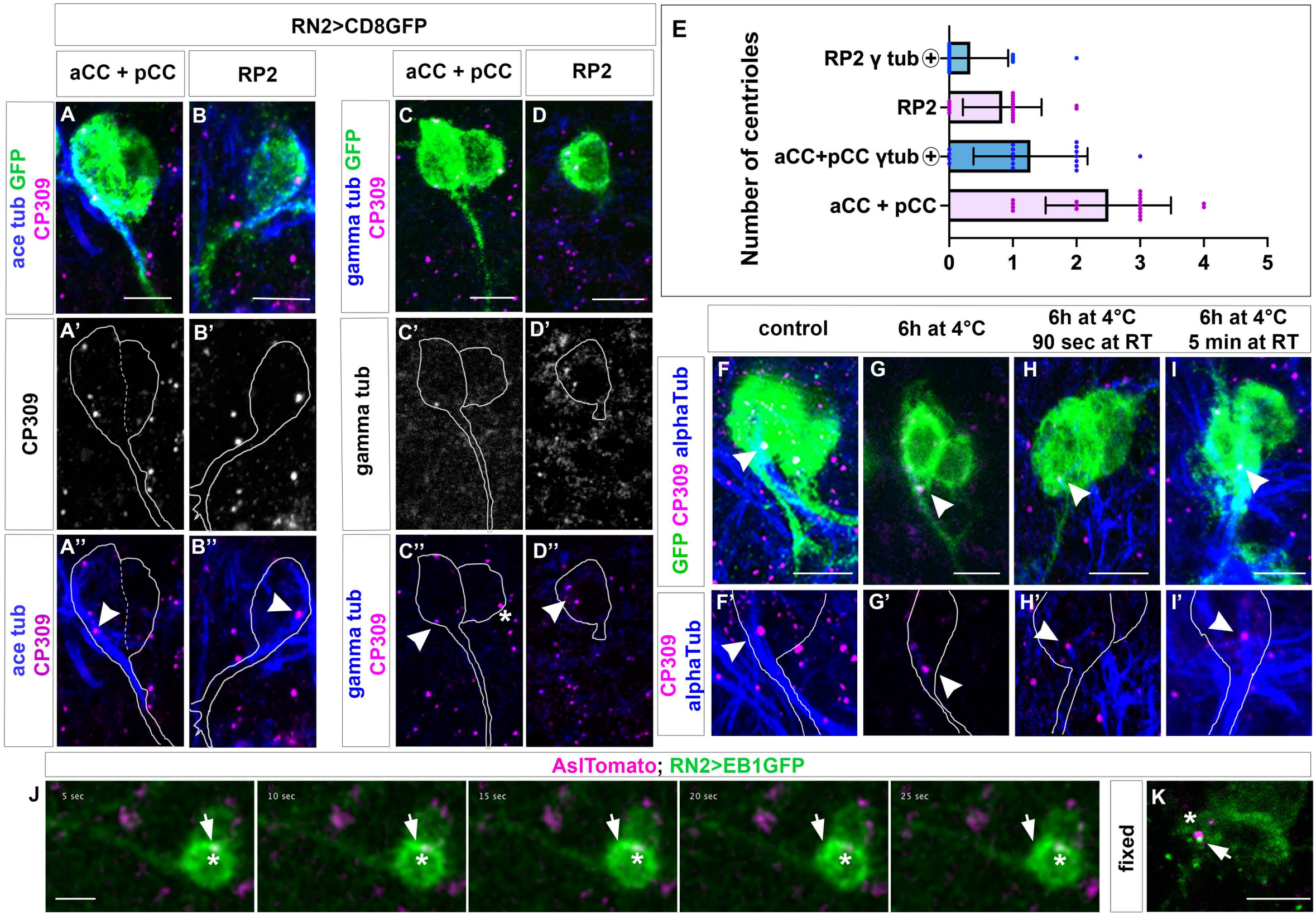
RN2>CD8GFP
aCC + pCC
RP2
aCC + pCC
RP2
ace tub GFP
CP309
gamma tub GFP
CP309
CP309
gamma tub
ace tub
CP309
gamma tub
CP309
A
B
C
D
A'
B'
C'
D'
A''
B''
C''
D''
E
Number of centrioles
RP2 γ tub ⊕
RP2
aCC+pCC γtub ⊕
aCC + pCC
0
1
2
3
4
5
control
6h at 4°C
6h at 4°C
90 sec at RT
6h at 4°C
5 min at RT
GFP CP309 alphaTub
CP309
alphaTub
F
G
H
I
F'
G'
H'
I'
AslTomato; RN2>EB1GFP
J
5 sec
10 sec
15 sec
20 sec
25 sec
fixed
K

Fig. 6

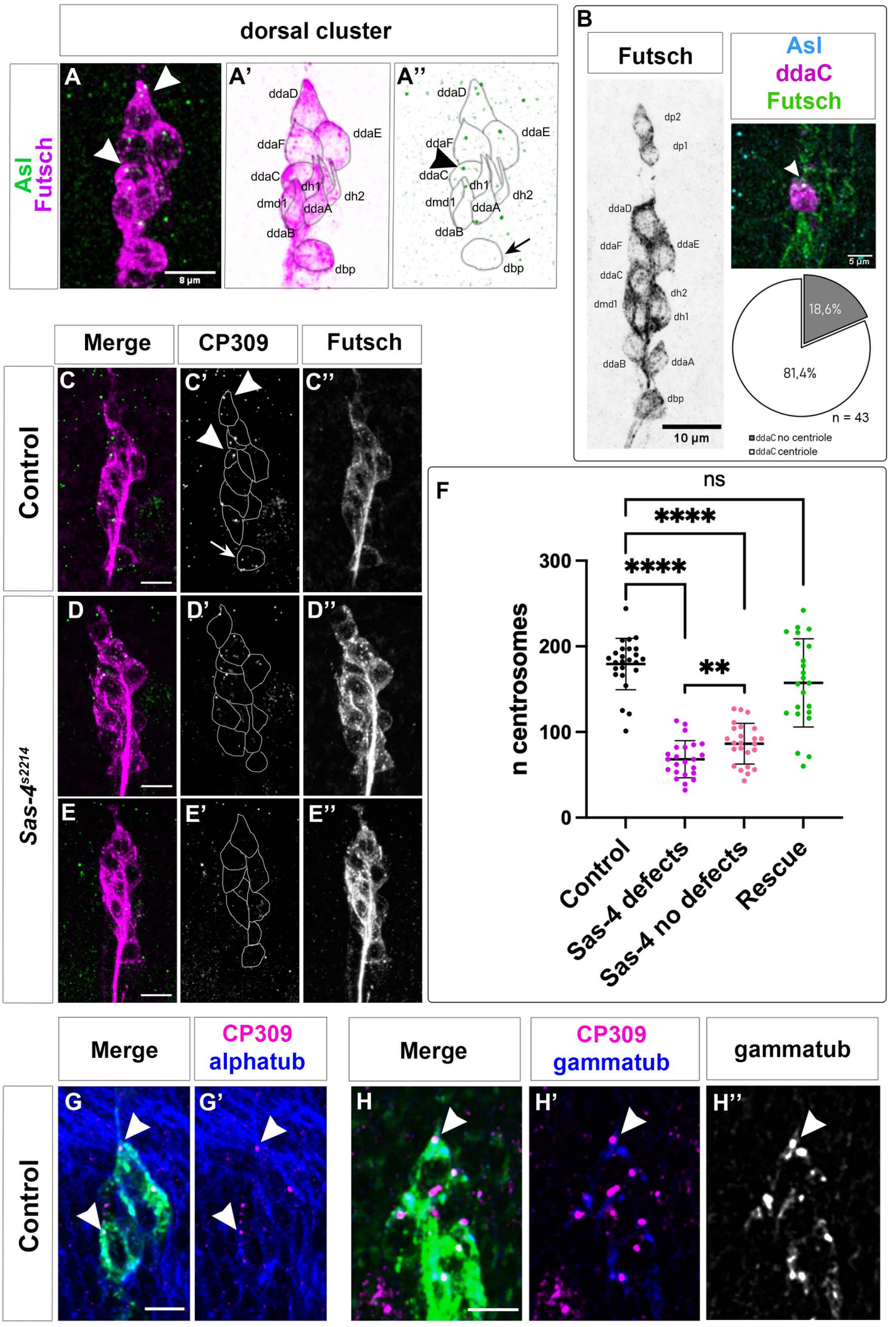
dorsal cluster
Asl
Futsch
A
A'
A''
ddaD
ddaE
ddaF
ddaC
dh1
dh2
dmd1
ddaA
ddaB
dbp
8 µm
B
Futsch
Asl
ddaC
Futsch
dp2
dp1
10 µm
5 µm
18,6%
81,4%
n = 43
ddaC no centriole
ddaC centriole
Merge
CP309
Futsch
Control
Sas-4s2214
C
C'
C''
D
D'
D''
E
E'
E''
F
ns
****
****
**
n centrosomes
300
200
100
0
Control
Sas-4 defects
Sas-4 no defects
Rescue
Merge
CP309
alphatub
Merge
CP309
gammatub
gammatub
Control
G
G'
H
H'
H''

Fig. 7

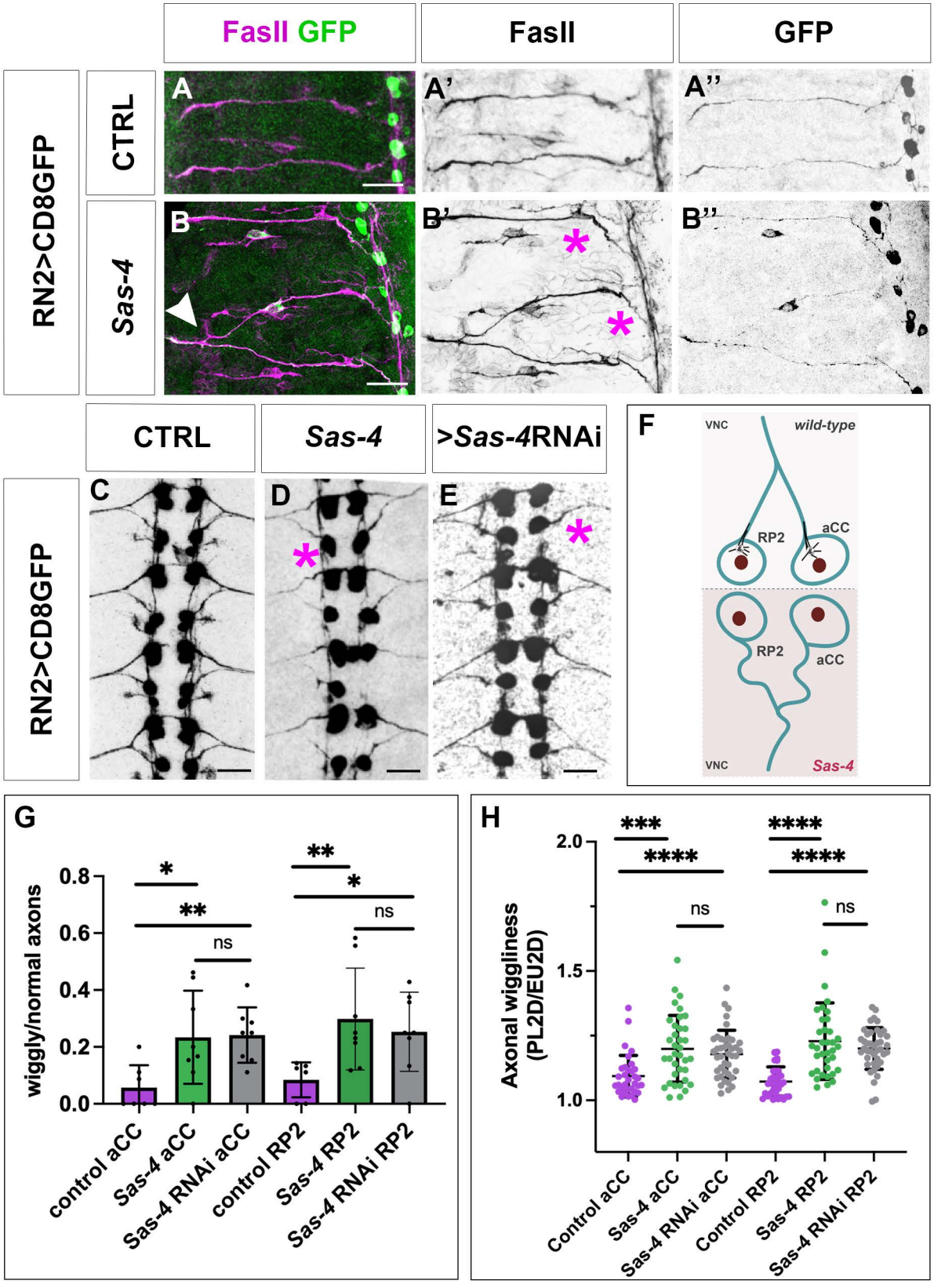
FasII GFP
FasII
GFP
RN2>CD8GFP
CTRL
Sas-4
A
A'
A''
B
B'
B''
CTRL
Sas-4
>Sas-4RNAi
C
D
E
F
VNC
wild-type
RP2
aCC
Sas-4
G
wiggly/normal axons
control aCC
Sas-4 aCC
Sas-4 RNAi aCC
control RP2
Sas-4 RP2
Sas-4 RNAi RP2
ns
H
Axonal wiggliness (PL2D/EU2D)
Control aCC
Sas-4 aCC
Sas-4 RNAi aCC
Control RP2
Sas-4 RP2
Sas-4 RNAi RP2
ns

Fig. 8

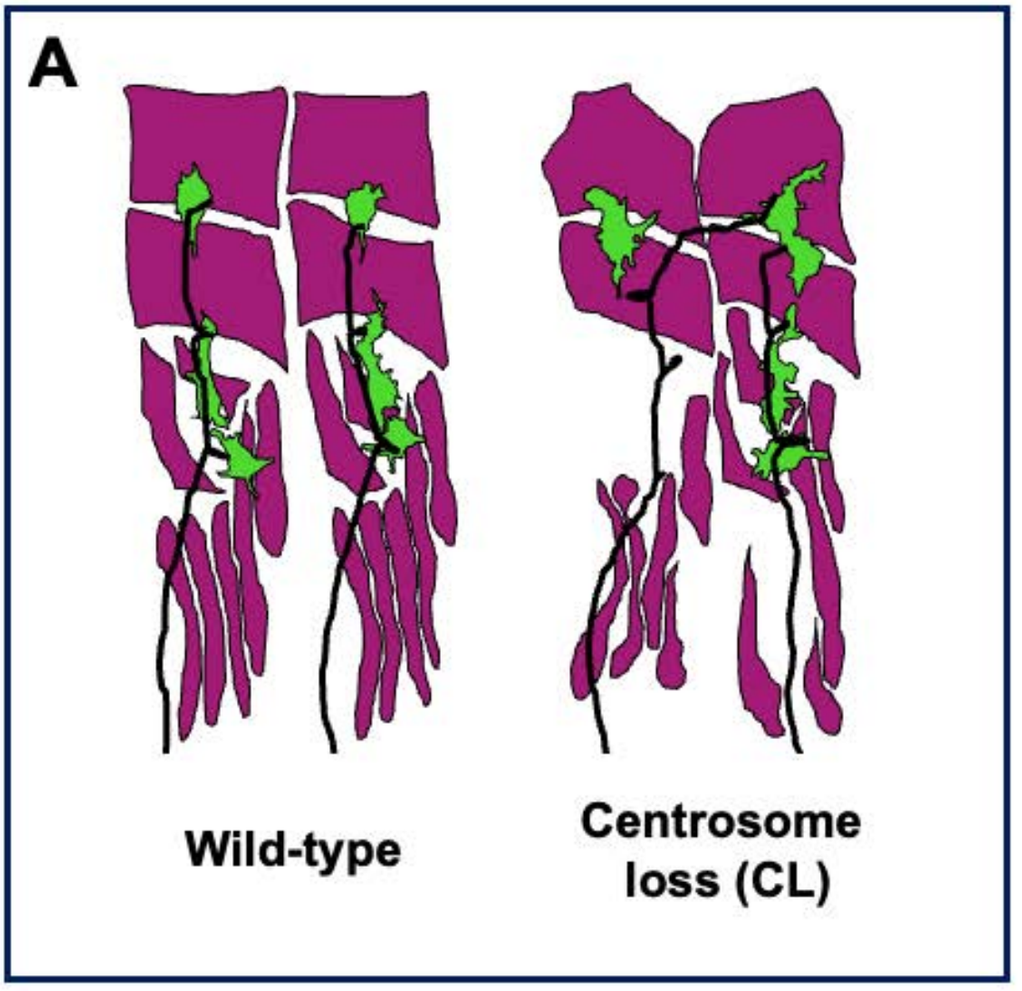
A
Wild-type
Centrosome loss (CL)

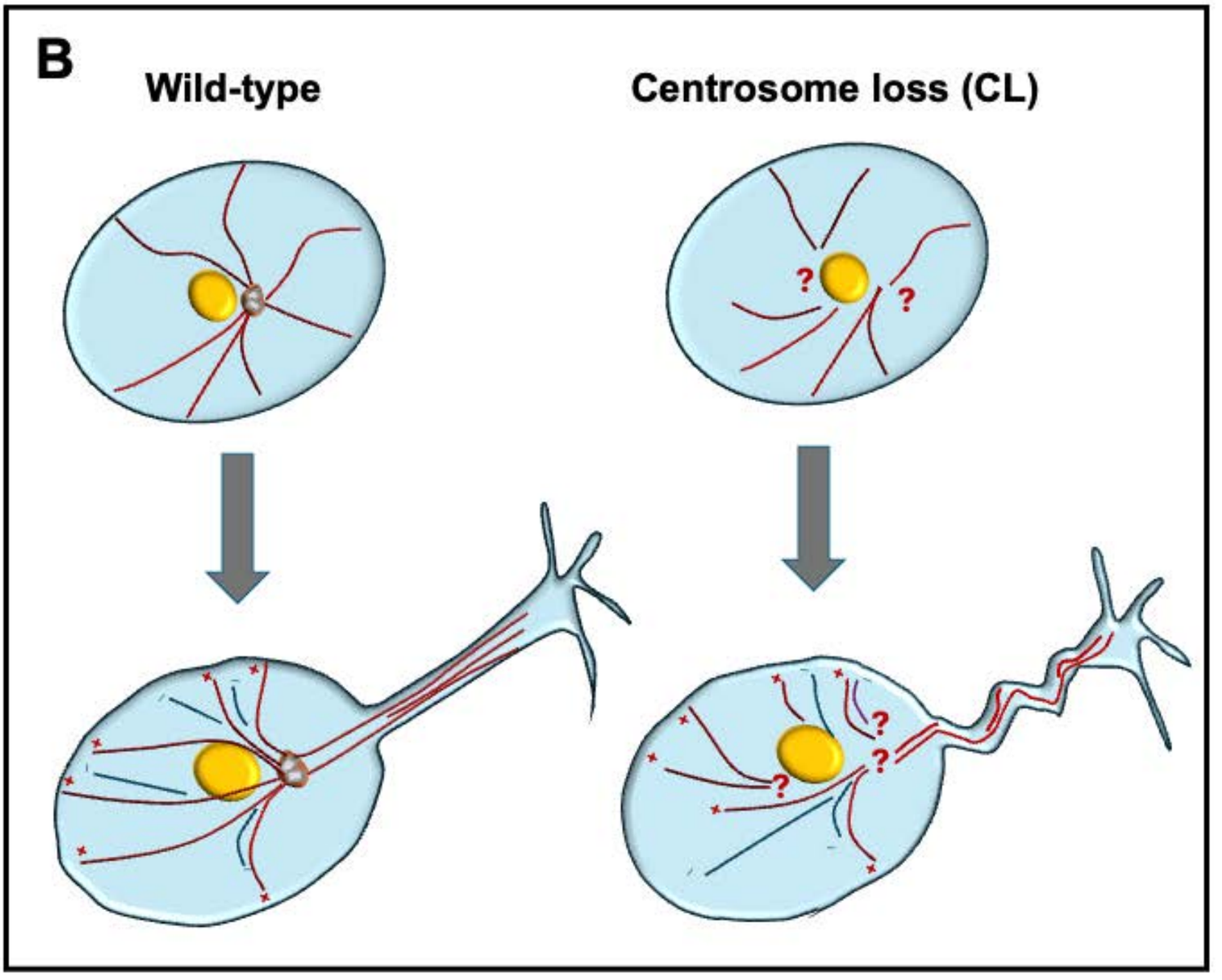
B
Wild-type
Centrosome loss (CL)
?
?
?
?
?

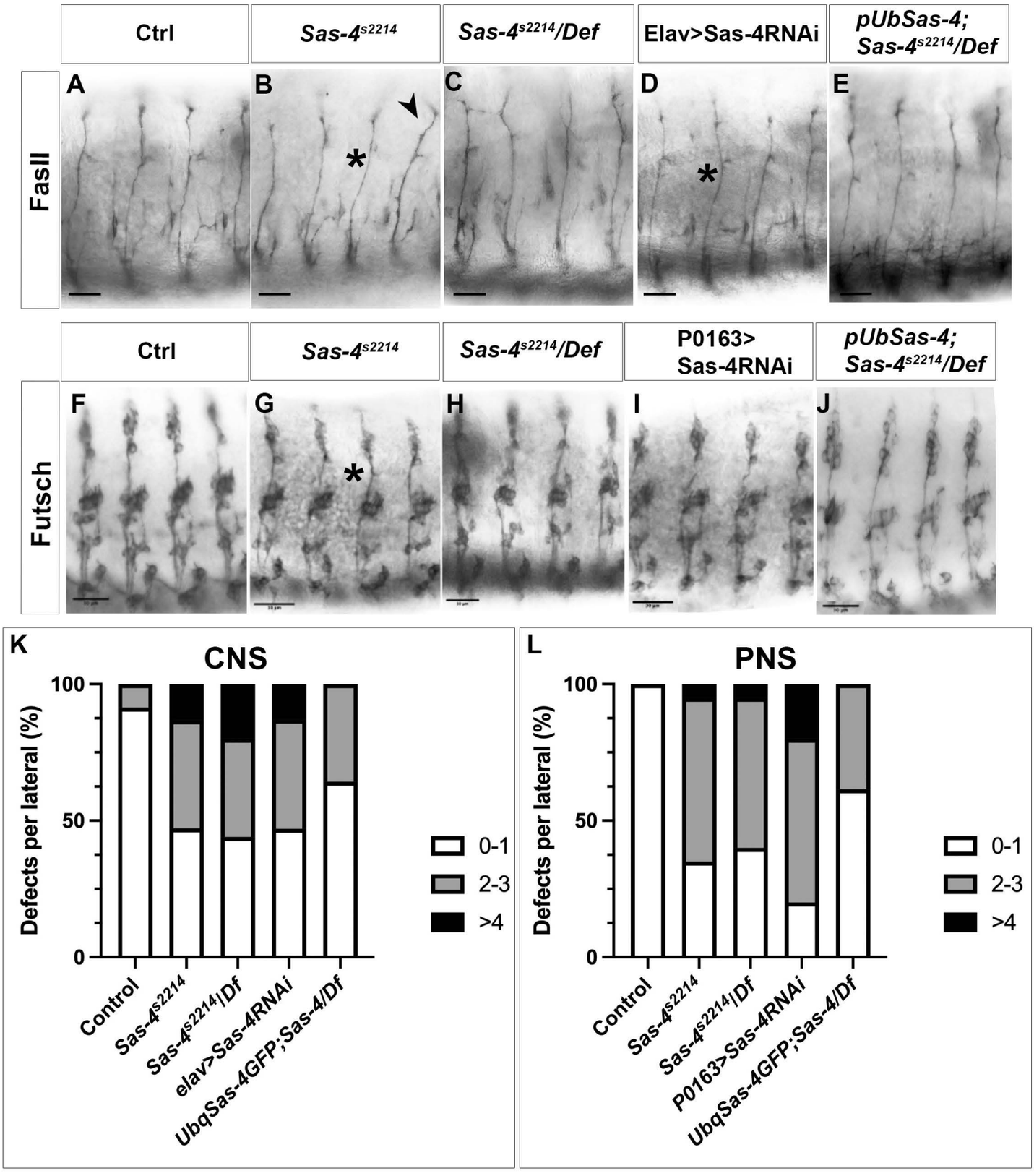
Ctrl
Sas-4s2214
Sas-4s2214/Def
Elav>Sas-4RNAi
pUbSas-4; Sas-4s2214/Def
FasII
A
B
C
D
E
Ctrl
Sas-4s2214
Sas-4s2214/Def
P0163> Sas-4RNAi
pUbSas-4; Sas-4s2214/Def
Futsch
F
G
H
I
J
K
CNS
Defects per lateral (%)
100
50
0
Control
Sas-4s2214
Sas-4s2214|Df
elav>Sas-4RNAi
UbqSas-4GFP;Sas-4/Df
0-1
2-3
>4
L
PNS
Defects per lateral (%)
100
50
0
Control
Sas-4s2214
Sas-4s2214|Df
P0163>Sas-4RNAi
UbqSas-4GFP;Sas-4/Df
0-1
2-3
>4

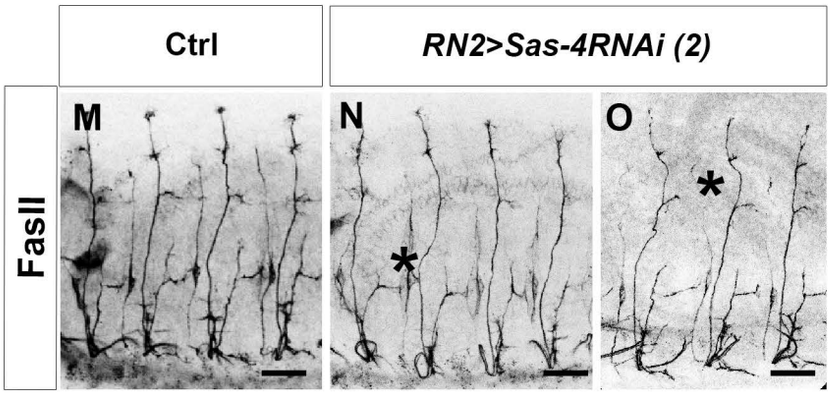
Ctrl
RN2>Sas-4RNAi (2)
FasII
M
N
O

Sup. Fig 2

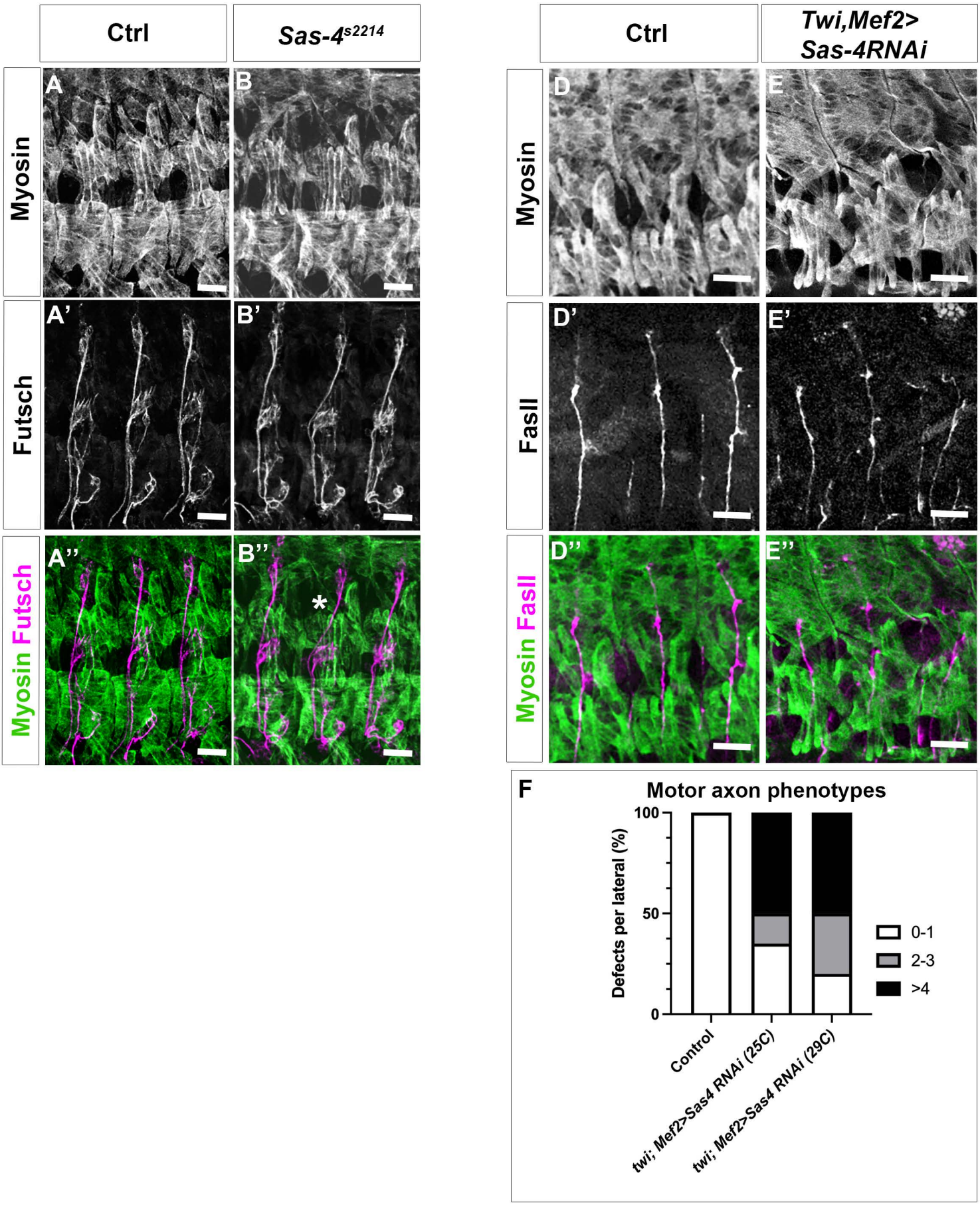
Ctrl
Sas-4s2214
Ctrl
Twi,Mef2>
Sas-4RNAi
Myosin
Futsch
Myosin Futsch
Myosin
FasII
Myosin FasII
A
B
A'
B'
A''
B''
*
D
E
D'
E'
D''
E''
F
Motor axon phenotypes
Defects per lateral (%)
100
50
0
0-1
2-3
>4
Control
twi; Mef2>Sas4 RNAi (25C)
twi; Mef2>Sas4 RNAi (29C)

Sup. Fig 3

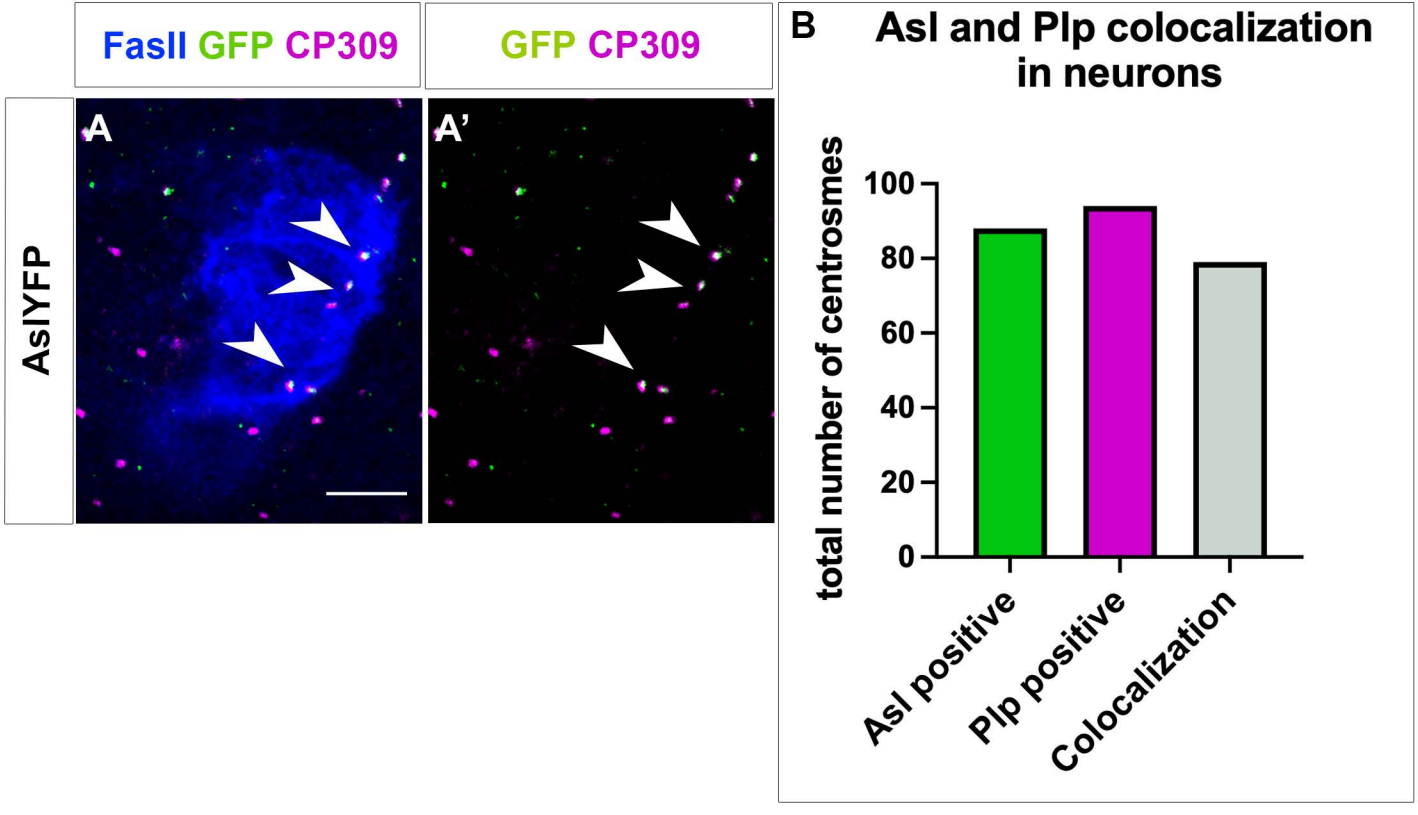
FasII GFP CP309
GFP CP309
AslYFP
A
A'
B
Asl and Plp colocalization in neurons
total number of centrosmes
100
80
60
40
20
0
Asl positive
Plp positive
Colocalization
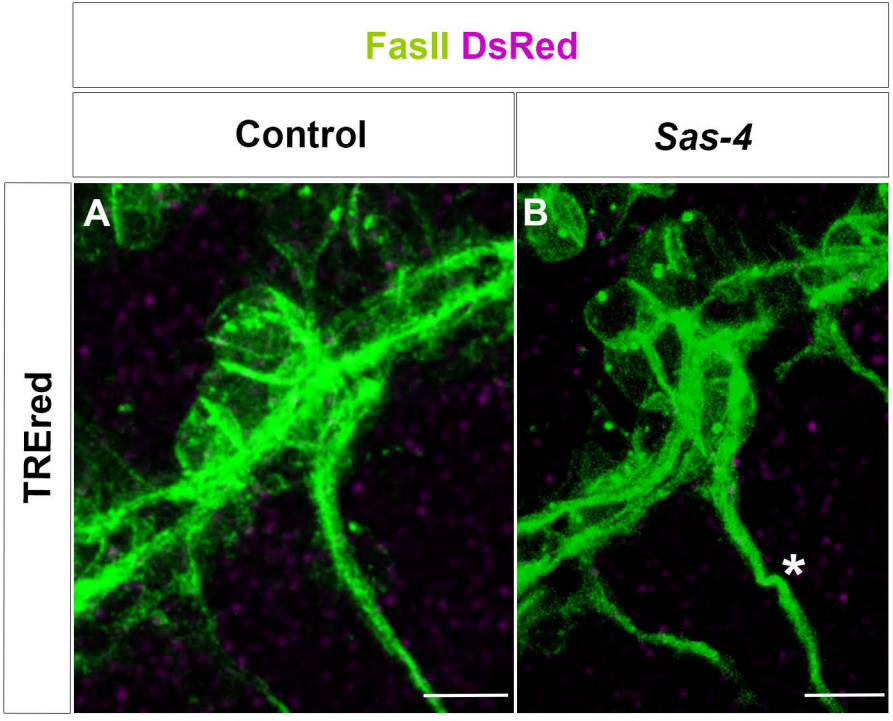
Sup. Fig 4